

# An endosomal syntaxin and the AP-3 complex are required for formation and maturation of candidate lysosome-related secretory organelles (mucocysts) in *Tetrahymena thermophila*

Harsimran Kaur<sup>a</sup>, Daniela Sparvoli<sup>a</sup>, Hiroko Osakada<sup>b</sup>, Masaaki Iwamoto<sup>b</sup>, Tokuko Haraguchi<sup>b,c</sup>, and Aaron P. Turkewitz<sup>a,\*</sup>

<sup>a</sup>Department of Molecular Genetics and Cell Biology, University of Chicago, Chicago, IL 60637; <sup>b</sup>Advanced ICT Research Institute, National Institute of Information and Communications Technology, Kobe 651-2492, Japan;

<sup>c</sup>Graduate School of Frontier Biosciences, Osaka University, Suita 565-0871, Japan

**ABSTRACT** The ciliate *Tetrahymena thermophila* synthesizes large secretory vesicles called mucocysts. Mucocyst biosynthesis shares features with dense core granules (DCGs) in animal cells, including proteolytic processing of cargo proteins during maturation. However, other molecular features have suggested relatedness to lysosome-related organelles (LROs). LROs, which include diverse organelles in animals, are formed via convergence of secretory and endocytic trafficking. Here we analyzed *Tetrahymena* syntaxin 7-like 1 (Stx7l1p), a Qa-SNARE whose homologues in other lineages are linked with vacuoles/LROs. Stx7l1p is targeted to both immature and mature mucocysts and is essential in mucocyst formation. In *STX7L1*-knockout cells, the two major classes of mucocyst cargo proteins localize independently, accumulating in largely nonoverlapping vesicles. Thus initial formation of immature mucocysts involves heterotypic fusion, in which a subset of mucocyst proteins is delivered via an endolysosomal compartment. Further, we show that subsequent maturation requires AP-3, a complex widely implicated in LRO formation. Knockout of the  $\mu$ -subunit gene does not impede delivery of any known mucocyst cargo but nonetheless arrests mucocyst maturation. Our data argue that secretory organelles in ciliates may represent a new class of LROs and reveal key roles of an endosomal syntaxin and AP-3 in the assembly of this complex compartment.

## Monitoring Editor

Adam Linstedt  
Carnegie Mellon University

Received: Jan 10, 2017

Revised: Mar 22, 2017

Accepted: Mar 28, 2017

## INTRODUCTION

Cells can respond to, and influence, changes in their environment via protein secretion. In eukaryotes, the predominant mechanism of protein secretion involves fusion of cytoplasmic vesicles with the plasma membrane, resulting in exocytic release of vesicle contents to the cell exterior (Palade, 1975; Keller and Simons, 1997). The

secreted molecules, control of exocytic fusion, and features of secretory vesicles have been elaborated over evolutionary time. In animals, for example, two prominent pathways allow sorting of specific subsets of secretory proteins, which are concentrated for storage in distinct vesicular compartments and finally released via tightly regulated exocytosis. The first pathway generates dense core granules (DCGs) and is best known for controlled insulin secretion (Roder *et al.*, 2016). A key step occurs in the *trans*-Golgi network (TGN) with the heterotypic coaggregation of specific soluble proteins destined for DCGs. These proteins associate with membrane proteins and lipids, which, in some as poorly understood way, directs the ensemble to budding immature DCGs (Orci *et al.*, 1987; Chanat and Huttner, 1991; Arvan and Castle, 1998; Tanguy *et al.*, 2016). Immature DCGs are subsequently matured by steps including homotypic fusion, reorganization via proteolytic processing of condensed cargo proteins, and retrieval of both missorted soluble constituents and secretory granule maturation factors via clathrin-coated vesicles

This article was published online ahead of print in MBoC in Press (<http://www.molbiolcell.org/cgi/doi/10.1091/mbc.E17-01-0018>) on April 5, 2017.

\*Address correspondence to: Aaron Turkewitz ([apturkew@midway.uchicago.edu](mailto:apturkew@midway.uchicago.edu)).  
Abbreviations used: DCG, dense core granule; GRL, granule lattice; GRT, granule tip; HOPS, homotypic fusion and protein sorting complex; Igr, induced upon granule regeneration; LRO, lysosome-related organelle; VPS10, vacuolar protein sorting 10.

© 2017 Kaur *et al.* This article is distributed by The American Society for Cell Biology under license from the author(s). Two months after publication it is available to the public under an Attribution–Noncommercial–Share Alike 3.0 Unported Creative Commons License (<http://creativecommons.org/licenses/by-nc-sa/3.0>).

“ASCB®” “The American Society for Cell Biology®,” and “Molecular Biology of the Cell®” are registered trademarks of The American Society for Cell Biology.

(Docherty and Steiner, 1982; Orci et al., 1985; Tooze, 1991; Kuliawat et al., 1997; Molinete et al., 2000; Morvan and Tooze, 2008).

A second distinct class of secretory structures is made up of lysosome-related organelles (LROs), including pigment granules (melanosomes), Weibel–Palade bodies, and T-cell lytic granules in animals (Marks et al., 2013). LROs, like DCGs, contain cargo exported from the TGN, and such cargo proteins in some cases assemble into large macromolecular complexes during transport in the secretory pathway (Hannah et al., 2002). However, in contrast with DCGs, a subset of LRO proteins are acquired via trafficking from endosomes, and thus LROs (like lysosomes) arise from a combination of secretory and endocytic trafficking (Raposo et al., 2007). Indeed, the formation of LROs relies on proteins and mechanisms that substantially overlap with mechanisms involved in lysosome formation (Bonifacino, 2004; Luzio et al., 2014). The mechanisms by which cells have adapted lysosome-related machinery to generate such a wide range of LROs and target specific proteins to LROs versus classical lysosomes are incompletely understood. Proteins involved in LRO formation include the AP-3 adaptor, the homotypic fusion and protein sorting (HOPS) complex, Rab32 and Rab38, and three biogenesis of LROs complex (BLOC) complexes (Starcevic et al., 2002; Li et al., 2003; Gautam et al., 2006; Wasmeyer et al., 2006). For example, the AP-3 complex mediates cargo sorting to mouse melanosomes, *Drosophila* eye pigment granules, and *Caenorhabditis elegans* gut granules (Kantheti et al., 1998; Mullins et al., 2000; Hermann et al., 2005).

Although both DCGs and LROs play key roles in animal cell physiology, relatively little is established regarding their distribution and significance in other eukaryotic lineages. DCGs, as defined in animals, are likely restricted to that lineage because some key determinants, such as the prohormone convertases, appear unique to animals (Steiner, 1998). The situation is different for LROs, in that the AP-3 adaptor and HOPS complex are widely conserved (Dacks et al., 2008; Klinger et al., 2013). Plant cells, for example, contain multiple classes of vacuoles, some of which depend on AP-3 (Feraru et al., 2010; Zwiewka et al., 2011; Blaby-Haas and Merchant, 2014). However, AP-3 involvement does not unequivocally define LROs because AP-3 may contribute to other pathways, including classical DCGs (Grabner et al., 2006; Asensio et al., 2010).

Strongly supported LRO candidates are the specialized secretory organelles in Apicomplexan parasites. In *Toxoplasma gondii*, the formation of rhoptries and micronemes, and perhaps the dense granules, involves HOPS complex subunits and a receptor in the vacuolar protein sorting 10 (VPS10)/sortilin family (Sloves et al., 2012; Morlon-Guyot et al., 2015). This family of receptors was first defined in budding yeast, where VPS10 is involved in protein trafficking to vacuoles, and the related sortilin receptors in animals transport cargo to lysosomes and LROs (Marcusson et al., 1994; Canuel et al., 2009). Acidocalcisomes, whose formation requires AP-3, may be a further example of an LRO (Docampo et al., 2005, 2013).

Ciliates are a sister clade to the mainly parasitic apicomplexans, both falling within the alveolate lineage (Gao et al., 2016). In many ciliates, exocytic secretion from large vesicles facilitates predation or predator defense, encystment, and other functions (Wessenberg and Antipa, 1970; Rosati and Modeo, 2003). Formation and exocytosis of the vesicles have been studied at the molecular level in *Tetrahymena thermophila* and *Paramecium tetraurelia*, where they are known as mucocysts and trichocysts, respectively, and bear many similarities to animal DCGs, including aggregation of cargo proteins and subsequent proteolytic processing during maturation (Collins and Wilhelm, 1981; Adoutte et al., 1984; Vayssie et al., 2000; Turkewitz, 2004; Rahaman et al., 2009). However, neither the

major core proteins nor the processing enzymes involved in maturation are related to those in DCGs (Madeddu et al., 1995; Kumar et al., 2014, 2015; Guerrier et al., 2017). In addition, the formation of ciliate secretory vesicles includes features that are significantly different from that of DCGs, judging by electron microscopy. Studies of trichocyst formation in the ciliate *Pseudomicrothorax dubius* revealed a post-Golgi step in which two morphologically distinct classes of vesicles underwent fusion (Peck et al., 1993). This is not characteristic of DCG formation in animals.

Insight into mechanisms of secretory vesicle formation in ciliates has emerged from expression patterns of *Tetrahymena* genes encoding mucocyst cargo proteins. These cargo proteins belong principally to families called granule lattice (GRL) and granule tip (GRT) and are coregulated at the transcriptional level (Cowan et al., 2005; Bowman et al., 2005b; Rahaman et al., 2009). Analysis of additional coregulated genes led to the discovery that mucocyst formation requires *SOR4*, which encodes a receptor in the VPS10/sortilin family, and that *SOR4* is specifically required to target GRT proteins to mucocysts (Briguglio et al., 2013). Because receptors in this family are widely involved in protein sorting to LROs or lysosomes as just described, the role of *SOR4* in mucocyst formation suggested that the ciliate vesicles were evolutionarily related to LROs.

To better understand mucocyst biogenesis, we sought additional genes involved in their formation. AP-3 represents one candidate, and genes for AP-3 subunits in *T. thermophila* are coregulated with mucocyst-related genes (Briguglio et al., 2013). A second potentially informative gene family is made up of the soluble *N*-ethylmaleimide-sensitive factor attachment protein receptors (SNAREs; Sollner et al., 1993). The Qa class of SNAREs, also called syntaxins, contains five subfamilies (Bennett et al., 1993). Those in subclass Qa.III.b, including mammalian syntaxin 7 and 13 and budding yeast Pep12p and Vam3p, reside on endosomes and are involved in endolysosomal trafficking (Klopper et al., 2007). Syntaxin 7 mediates trafficking from late endosomes to lysosomes; syntaxin 13 resides in tubular early and recycling endosomes, and its knockdown impairs cargo transport to melanosomes (Mullock et al., 2000; Jani et al., 2015), although it does not appear to be involved in fusion of carriers with melanosomes per se (Dennis et al., 2015). *Saccharomyces cerevisiae* Pep12p and Vam3p are required for transport of newly synthesized proteins to the vacuole via two distinct pathways. Pep12p is localized to the prevacuolar endosome, where it functions in the fusion of Golgi-derived transport vesicles through the carboxypeptidase Y (CPY) pathway (Becherer et al., 1996). Vam3p is localized to the vacuole, where it mediates delivery of cargoes from both the CPY and alkaline phosphatase pathways (Wada et al., 1997).

In work described here, we assessed the roles of an endolysosomal Qa-SNARE and AP-3. Each is required for mucocyst biogenesis, and targeted gene-knockout strains accumulate distinct arrested mucocyst intermediates. These arrested intermediates are consistent with a critical role for the SNARE in homotypic and heterotypic vesicle fusion during immature mucocyst formation, whereas AP-3 is instead required for mucocyst maturation. These results strongly support the idea that mucocyst biogenesis in *T. thermophila* depends on machinery associated with LROs.

## RESULTS

### The *T. thermophila* AP-3 complex is coexpressed with known mucocyst-associated genes

The AP-3 complex is involved in sorting to LROs, including vacuoles in *S. cerevisiae* and melanosomes in mice. Of interest, genes encoding subunits of the AP-3 complex appear to be coregulated in *T. thermophila* with genes linked to mucocyst biosynthesis, an

observation derived from genome-wide expression data (*Tetrahymena* Functional Genomics Database [TFGD]; <http://tfgd.ihb.ac.cn>; Xiong *et al.*, 2011). Expression profiles are shown in Figure 1 for the gene encoding the AP-3  $\mu$  subunit, called *APM3*, together with a set of other genes encoding known mucocyst determinants (sorting receptor: *SOR4*; cargo proteins: *GRT1* and *GRL3*; processing enzymes: *CTH3* and *CTH4*; Figure 1A), as well as several genes involved at other steps of membrane trafficking (endoplasmic reticulum translocation: *SEC61*; Golgi trafficking: *COP1*; clathrin-mediated coat formation: *CHC1*; Figure 1B). Four other AP complexes are present in *T. thermophila*: two AP-1 complexes, AP-2, and AP-4 (Supplemental Figure S1). In contrast to the AP-3  $\mu$ -subunit gene, the genes encoding the  $\mu$  subunits of these other complexes show different expression patterns (Figure 1B) and are not judged, in the TFGD, to be coregulated with mucocyst-associated genes.

### AP-3 is nonessential in *T. thermophila*

To investigate the cellular functions of *APM3*, including a potential role of AP-3 in mucocyst biogenesis, we targeted the macronuclear *APM3* locus for homologous recombination with a drug-resistance cassette (Supplemental Figure S2A). With this standard approach, all ~45 copies of a gene in the polyploid macronucleus can be replaced with the cassette during roughly 3–4 wk of selection, producing a functional knockout if the gene is nonessential (Cassidy-Hanley *et al.*, 1997). We generated the *APM3*-knockout line, called  $\Delta apm3$ , and assayed for the presence of the gene transcript by reverse transcription PCR (RT-PCR). There was no detectable *APM3* transcript in the knockout line (Supplemental Figure S2B), and *APM3* can therefore be considered a nonessential gene. In budding yeast and *Drosophila*, loss of the AP-3  $\mu$  subunit is sufficient to block AP-3-dependent activity (Cowles *et al.*, 1997; Stepp *et al.*, 1997; Mullins *et al.*, 2000), so we infer that the AP-3 complex is nonessential in *Tetrahymena*. Indeed, *Tetrahymena* lines lacking *APM3* showed no growth defects under standard laboratory culture conditions. Of interest, results from parallel targeting of other AP  $\mu$  subunits in *Tetrahymena* suggested that the AP-1A, AP-2, and AP-4 complexes are essential in this organism because these genes could not be replaced in the macronucleus (unpublished data).

### *APM3* is required to form mature mucocysts

To examine whether *APM3* is required for mucocyst formation and/or exocytosis, we first tested the secretory response of  $\Delta apm3$  in response to dibucaine, which triggers synchronous mucocyst exocytosis (Satir, 1977). When wild-type cells are exposed briefly to dibucaine, the mucocyst contents are released as macroscopic protein aggregates and can be visualized after low-speed centrifugation as a thick, flocculent layer (Figure 2A, lower left). In contrast,  $\Delta apm3$  cells did not release any pelletable flocculent (Figure 2A, lower right).

The  $\Delta apm3$  secretion phenotype is comparable to previously characterized mutants, which were divided into subclasses based on their defects in mucocyst formation, transport/docking, or exocytosis (Orias *et al.*, 1983; Melia *et al.*, 1998; Bowman *et al.*, 2005a). All characterized mutants with defects in mucocyst formation per se accumulate mucocyst protein precursors rather than the processed forms generated during mucocyst maturation (Ding *et al.*, 1991; Turkewitz *et al.*, 1991; Melia *et al.*, 1998). Significantly, we found that mucocyst protein precursors accumulated in  $\Delta apm3$ . We analyzed cell lysates of wild-type and  $\Delta apm3$  cells by Western blotting with an antibody against mucocyst core protein Gr1p. Wild-type cells accumulated Gr1p predominantly in the fully processed form. In contrast, most Gr1p in  $\Delta apm3$  was present in the unprocessed form, although some fully processed Gr1p was also

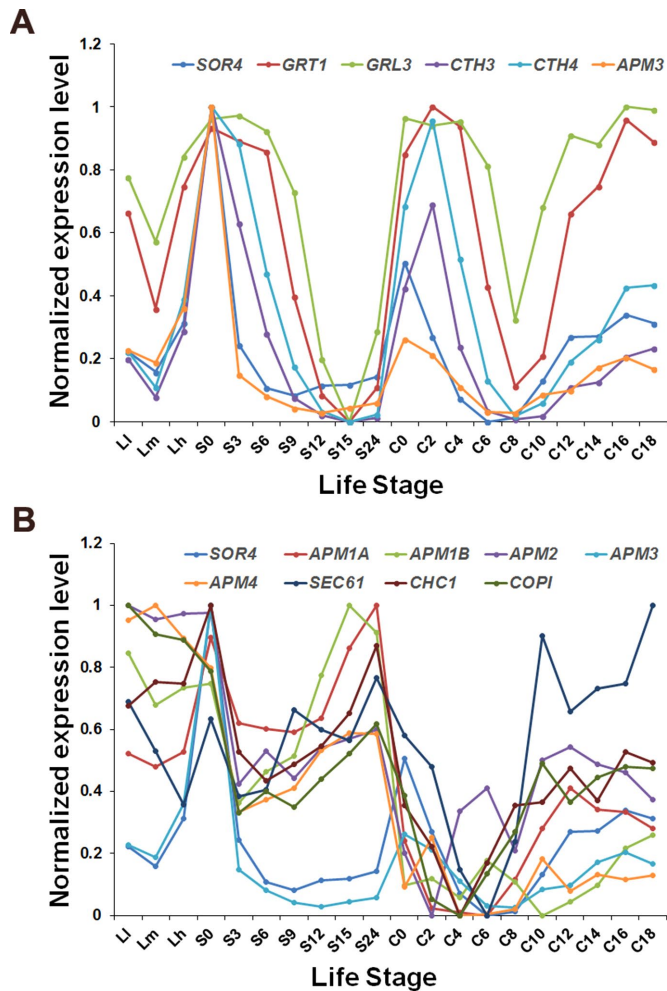


**FIGURE 1:** Expression profiling suggests a role for AP-3 adaptor complex in mucocyst biogenesis. (A) The gene encoding the AP-3 adaptor complex medium ( $\mu$ ) subunit (*APM3*) is coregulated with mucocyst-associated genes *SOR4*, *CTH3*, *CTH4*, *GRT1*, and *GRL3*, as judged by the similarity between their expression profiles. Expression profiles derived from sampling various culture conditions and analyzed via whole-genome microarrays were downloaded from the TFGD. They were plotted after normalizing each trace to that gene's maximum expression level. Points on the X-axis correspond to successive time points and represent growing, starved, and mating cultures, including three different culture densities (low [Li], medium [Lm], and high [Lh]); seven samples taken during 24 h of starvation (S0–S24), and 10 samples subsequently taken during 18 h after conjugation (C0–C18). More information on sampling and other conditions is given in Miao *et al.* (2009). (B) *T. thermophila* expresses the AP-1A, AP-1B, AP-2, and AP-4 adaptor complexes, but these show expression profiles distinct from those of mucocyst-associated genes. Expression profiles of a set of genes involved at other steps in protein secretion are also shown: *SEC61* (ER translocon subunit), *CHC1* (clathrin-coated pit component), and *COPI* (Golgi trafficking).

visible (Figure 2B). This processing defect indicates that the knockout cells have a defect in formation of mature mucocysts.

### $\Delta apm3$ cells accumulate cytoplasmic free and plasma membrane-docked immature mucocysts

To understand more fully the defect in  $\Delta apm3$ , we localized the mucocyst luminal proteins Gr13p and Gr1p by indirect immunofluorescence in fixed cells. In wild-type cells, these proteins accumulate

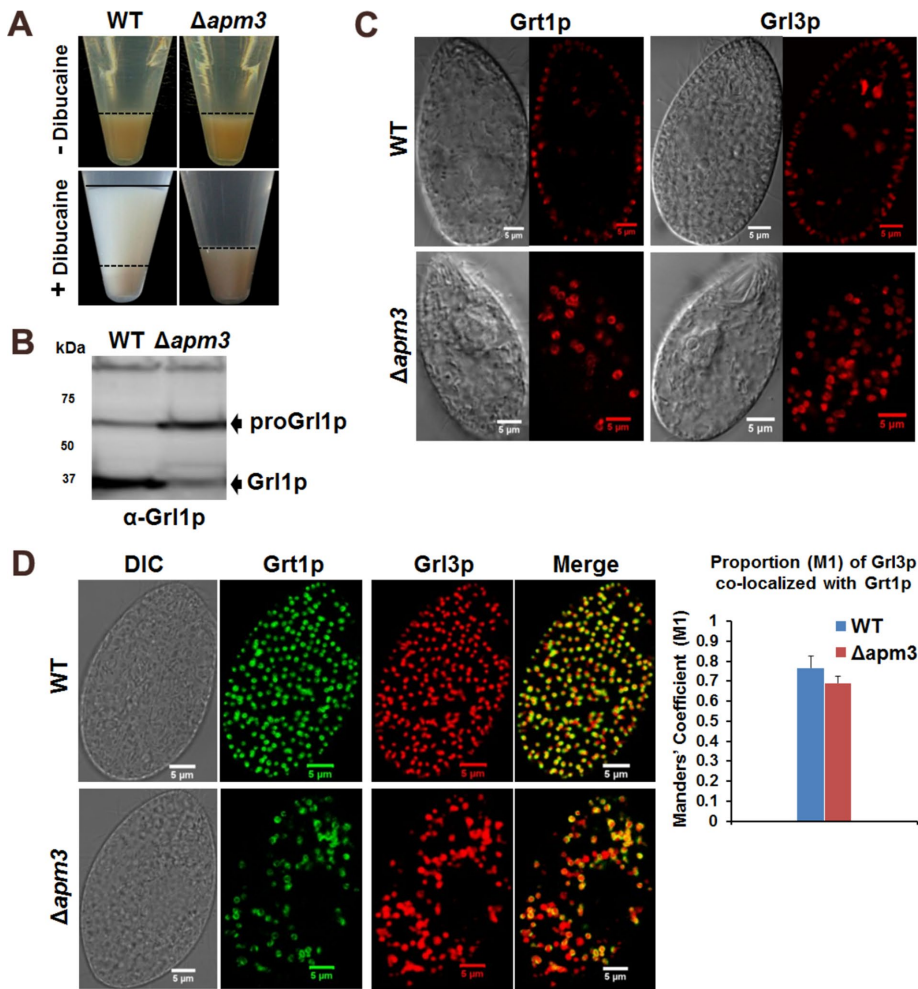


**FIGURE 2:** Knockout of the AP-3  $\mu$ -subunit gene disrupts mucocyst maturation. (A)  $\Delta apm3$  fails to release mucocyst contents. Identical numbers of stationary wild-type (WT) and  $\Delta apm3$  were exposed to dibucaine to stimulate mucocyst exocytosis. Samples were then centrifuged to produce a pellet of cells (dashed line) with an overlying flocculent layer (top and bottom, solid and dashed line respectively). In contrast to the WT sample, stimulated  $\Delta apm3$  show no flocculent layer. The poststimulation WT cell pellet is smaller than the  $\Delta apm3$  pellet because some WT cells are trapped in the sticky flocculent. Unstimulated WT and  $\Delta apm3$  are also shown. (B)  $\Delta apm3$  cells are partially inhibited in proGrl processing. Whole-cell lysates of WT and  $\Delta apm3$  were resolved by SDS-PAGE (4–20%), electroblotted onto PVDF, and probed with an antibody against Grl1p, which undergoes proteolytic processing during mucocyst maturation. In WT lysates, Grl1p appears predominantly in its fully processed form. In  $\Delta apm3$  lysates, Grl1p appears primarily as the unprocessed precursor (proGrl1p). (C)  $\Delta apm3$  cells accumulate mucocyst proteins in cytoplasmic vesicles. Mucocyst cargo proteins Grt1p and Grl3p were immunolocalized in fixed, permeabilized cells using mAbs 4D11 and 5E9, respectively. Single optical slices near the cell midsection. In WT cells, both proteins localize to mucocysts docked at the cell periphery (top). The elongated shape of the mucocysts can be seen when Grl3p is visualized (top, right). In  $\Delta apm3$  cells, both proteins localize to spherical vesicles in the cell interior (bottom). (D) Grt1p and Grl3p colocalize in  $\Delta apm3$  vesicles. Fixed, permeabilized WT and  $\Delta apm3$  cells were labeled to simultaneously localize Grl3p and Grt1p, using mAbs 5E9 and 4D11 directly coupled to fluorophores. Single near-tangential optical sections to capture mucocysts or vesicles at or near the cell periphery. Scale bars, 5  $\mu$ m. The extent of overlap between Grt1p and Grl3p is shown on the right. Twenty-five nonoverlapping optical sections in each cell line were quantified using the Manders correlation coefficient M1, and a mean M1 value for each population was determined from the sample. M1 values for WT: mean, 0.76; SD, 0.06; for  $\Delta apm3$ : mean, 0.69; SD, 0.035;  $p < 0.05$  as determined by one-tailed t test. For Pearson's correlation analysis of the same data, see Supplemental Figure S7A.

exclusively in mature docked mucocysts (Figure 2C, top). In  $\Delta apm3$ , both proteins accumulate in a relatively homogeneous cohort of spherical cytoplasmic vesicles (Figure 2C, bottom). When simultane-

ously visualized, Grl3p and Grt1p show significant colocalization in  $\Delta apm3$  cells, albeit somewhat reduced compared with that in wild type (Figure 2D). We quantified the levels of Grt1p and Grl3p in wild type and  $\Delta apm3$  by flow cytometry. Grl3p shows 28% reduction in the mutant relative to wild type (Supplemental Figure 3A), whereas Grt1p is reduced in the mutant by 43% (Supplemental Figure S3B). The reduced accumulation of these proteins in  $\Delta apm3$  cells may contribute to the reduced colocalization measured in this mutant.

To determine whether other mucocyst components were also targeted to that compartment in  $\Delta apm3$  cells, we expressed GFP-tagged copies of two enzymes required for mucocyst maturation, Cth3p and Cth4p (Kumar et al., 2014, 2015). Both enzymes colocalized with Grl3p in wild-type and  $\Delta apm3$  cells (Figure 3, A and B). Only partial colocalization is expected in these experiments because the GFP-tagged proteins are inducibly expressed for 2 h and would not be expected to access the pool of preexisting mucocysts or arrested mucocyst intermediates. In parallel experiments, Sor4p showed minimal overlap with Grl3p and therefore provides a negative control (Supplemental Figure S2C). Taken together, these data are consistent with the idea that the Grl3p-bearing vesicles in  $\Delta apm3$  represent arrested mucocyst intermediates.

We visualized the mucocyst-related structures in  $\Delta apm3$  by electron microscopy. In wild-type cells, numerous elongated docked mucocysts are prominent (marked with asterisks in Figure 4A, top left), and the crystalline organization of the dense core can be seen in favorable sections (Figure 4A, top right). No wild-type mucocysts were detected in  $\Delta apm3$ , but the defective mucocysts were easily recognizable as relatively homogeneous large vesicles containing granular but amorphous contents and not present in wild-type cells (Figure 4A, bottom). Of interest, some of these arrested mucocyst intermediates were docked at the plasma membrane at sites where mature mucocysts would be docked in wild-type cells; one such docked vesicle is shown in the bottom left of Figure 4A, marked with an arrowhead. As judged by analysis of antibody-labeled cell midsections, docked mucocyst-related vesicles in  $\Delta apm3$  are less numerous than docked mucocysts in wild-type cells (Figure 4B). In contrast, the  $\Delta apm3$  cells contain a larger number of undocked mucocyst-related vesicles compared with undocked mucocysts in wild-type cells (Figure 4B). Because of this balance, the total number of docked plus undocked vesicles is similar in the mutant and wild type.

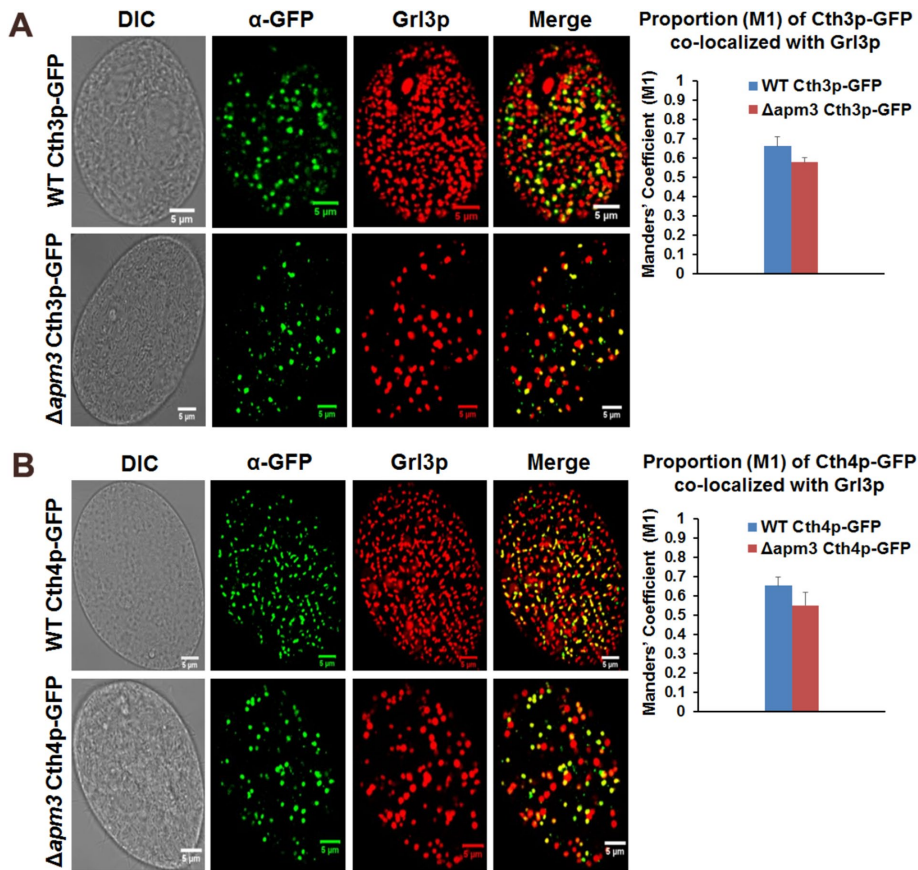


**FIGURE 3:** The Gr13p/Grt1p-bearing vesicles in  $\Delta apm3$  cells also contain key processing enzymes involved in mucocyst maturation. Transgene expression (*CTH3-GFP* or *CTH4-GFP*) was induced for 2 h with 2  $\mu\text{g/ml}$  CdCl<sub>2</sub> at 30°C, after which, cells were fixed, permeabilized, and immunolabeled to localize Gr13p (mAb 5E9) and GFP-tagged Cth3p or Cth4p (rabbit anti-GFP). Single optical sections. (A) Cth3p-GFP and Gr13p colocalize in WT (top) and  $\Delta apm3$  (bottom) cells. Scale bars, 5  $\mu\text{m}$ . (B) Cth4p-GFP and Gr13p colocalize in WT (top) and  $\Delta apm3$  (bottom). The extent of pairwise overlap was measured using 25 nonoverlapping optical sections for each cell line and is shown on the right. M1 values for WT Cth3p-GFP: mean, 0.66; SD, 0.048; for  $\Delta apm3$  Cth3p-GFP: mean, 0.58; SD, 0.026;  $p < 0.05$  as determined by one-tailed t test. M1 values for WT Cth4p-GFP: mean, 0.65; SD, 0.044; for  $\Delta apm3$  Cth4p-GFP: mean, 0.55; SD, 0.072;  $p < 0.05$  as determined by one-tailed t test. For Pearson's correlation analysis of the same data, see Supplemental Figure S7, B and C.

The AP-3 complex in *Tetrahymena* therefore appears to be required for mucocyst maturation. One possibility is that AP-3 is required for cargo selection during vesicle budding from immature mucocysts to selectively remove a subset of the proteins present. However, we favor the idea that AP-3 is required during vesicle budding from a different compartment to deliver one or more components to immature mucocysts. Determining the localization of AP-3 could help to distinguish between the two models. Unfortunately, GFP-tagged versions of Apm3p appeared to aggregate (unpublished data), and thus were uninformative regarding endogenous protein localization.

### *T. thermophila* STX7L1, a late endosomal syntaxin with a mucocyst-related expression profile, is nonessential.

In budding yeast, AP-3 is required for vacuolar delivery of the syntaxin Vam3p (Cowles *et al.*, 1997; Darsow *et al.*, 1998). We therefore sought to determine whether a VAM3 homologue is present in *Tetrahymena* and targeted to mucocysts potentially in an AP-3-dependent pathway. With *S. cerevisiae* VAM3 as a query, we used

PSI-BLAST and reciprocal BLAST searches, as well as a SNARE classification website (<http://bioinformatics.mpibpc.mpg.de/snare/index.jsp>), to identify two *T. thermophila* SNAREs that fall into the Qa.III.b subclass (Supplemental Figure S4A). One of these hits, THERM\_00420770, also returned VAM3 as the top hit by reciprocal PSI-BLAST against *S. cerevisiae*. Based on data in the TFGD (<http://tfgd.ihb.ac.cn>), THERM\_00420770, but not the other Qa.III.b-SNARE, has an expression profile similar to those of known mucocyst-associated genes, including APM3 (Figure 5). We named the gene *STX7L1* for syntaxin 7-like 1 because it is homologous, although not demonstrably orthologous, to STX7 in humans.

Using the same approach as with APM3, we targeted *STX7L1* for disruption and obtained a complete macronuclear knockout, as judged by RT-PCR (Supplemental Figure S4, B and C). Thus *STX7L1* is also nonessential. The  $\Delta stx7l1$  cells, like  $\Delta apm3$ , showed no growth defect under standard laboratory culture conditions.

### Stx711p-GFP localizes to both arrested immature and mature mucocysts

To determine the localization of Stx711p, we expressed it as a GFP fusion under the control of the inducible *MTT1* promoter (Shang *et al.*, 2002). Western blotting of cell lysates after 3 h of induction using an anti-GFP antibody showed a full-length fusion protein of the expected size (Supplemental Figure S5A). In live, immobilized wild-type cells, Stx711p-GFP localized to a set of linearly arrayed puncta at the cell surface, strongly suggesting that the protein accumulated in mucocysts (Supplemental Figure S5B). To confirm this, we labeled fixed, permeabilized cells with an

antibody against mucocyst protein Gr13p. Stx711p-GFP colocalized extensively with Gr13p in docked mucocysts (Figure 6, top) and cytoplasmic structures that may be intermediates in mucocyst maturation, most clearly seen in cell midsections (Figure 6, middle). Of interest, Stx711p-GFP also localized to the arrested immature mucocyst intermediates in  $\Delta apm3$  cells (Figure 6, bottom), indicating that AP-3 is not required for delivery of this syntaxin to mucocysts.

### STX7L1 is required for mucocyst biogenesis

To ask whether *STX7L1* was required for mucocyst function, we tested the secretory response of  $\Delta stx7l1$  in response to dibucaine as described. Like  $\Delta apm3$ ,  $\Delta stx7l1$  cells did not release any visible flocculent (Figure 7A, right). Moreover,  $\Delta stx7l1$  cells were also defective in processing of proGr1p. Indeed, the defect was more severe than in  $\Delta apm3$  because no processed Gr1p product was detectable in  $\Delta stx7l1$  lysates (Figure 7B). Thus a syntaxin predicted to be involved in endosomal trafficking is required to generate mature mucocysts in *Tetrahymena*.

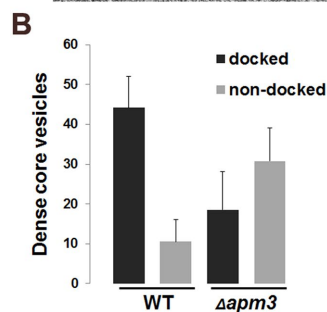
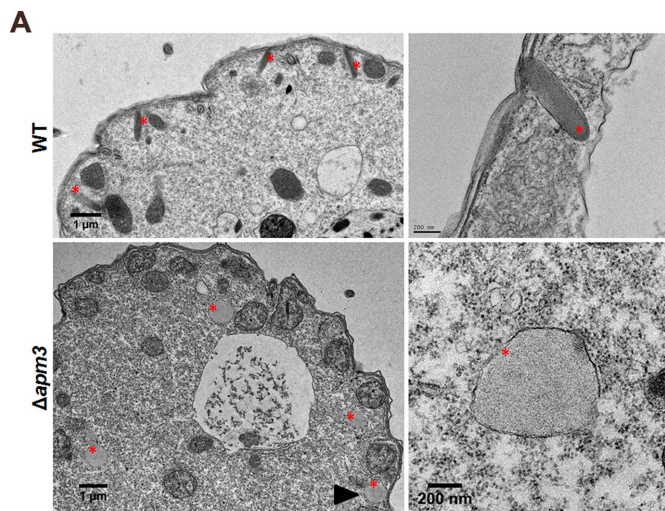


**FIGURE 4:** (A)  $\Delta apm3$  cells accumulate large vesicles with granular contents. In WT, numerous docked mucocysts (asterisks) are present (top, left) in which the cores are organized as elongated crystalline lattices (top, right). Scale bars, 1  $\mu\text{m}$  (left), 200 nm (right). In  $\Delta apm3$  cells, large vesicles with granular contents (asterisks) are found in the cytoplasm, with some docked at the plasma membrane. Scale bars, 1  $\mu\text{m}$  (left), 200 nm (right). A docked vesicle is marked with an arrowhead in the bottom left image. Scale bar, 1  $\mu\text{m}$ . (B) Quantification of mucocysts in WT vs. arrested mucocyst intermediates in  $\Delta apm3$ . As described in *Materials and Methods*, the Analyze Particles application of ImageJ was used to estimate docked vs. nondocked mucocysts/arrested intermediates in immunolabeled cell midsections, using six representative cells for each cell line. Docked vesicles: WT mean, 44.16, and SD = 7.78;  $\Delta apm3$  mean, 18.5, and SD, 9.6;  $p < 0.01$  as determined by one-tailed  $t$  test. Nondocked vesicles: WT mean, 10.5, and SD, 5.6;  $\Delta apm3$  mean, 30.83, and SD, 8.20;  $p < 0.01$  as determined by one-tailed  $t$  test. Mean of the total mucocysts/arrested mucocyst intermediates per cell: WT, 54.7;  $\Delta apm3$ , 49.3.

### Mucocyst cargo proteins in the GRL versus GRT families are separately targeted in $\Delta stx711$ but not $\Delta apm3$ cells

To better understand the defect in  $\Delta stx711$ , we observed cells using immunolabeling, live-cell imaging, and electron microscopy. First, we visualized proteins in the Grt and Grl families (Grt1p and Grl3p, respectively) by indirect immunofluorescence. Of interest, virtually no Grt1p could be detected in  $\Delta stx711$ , whereas Grl3p accumulated in heterogeneous cytoplasmic puncta (Supplemental Figure S5C, bottom). Consistent with these images, flow cytometry-based quantification revealed that Grl3p accumulation is somewhat reduced in  $\Delta stx711$  compared with wild type (20% reduction), whereas Grt1p is reduced by 95% in the mutant relative to wild type (Supplemental Figure S3, A and B).

The almost complete absence of Grt1p in  $\Delta stx711$  could indicate that this protein fails to accumulate in the mutant cells—for

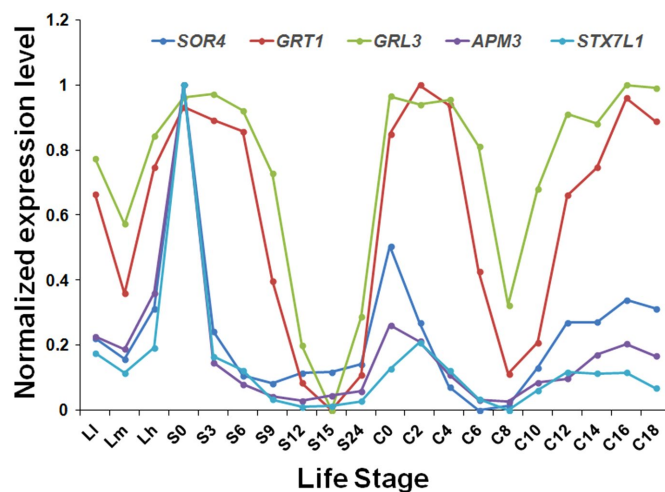
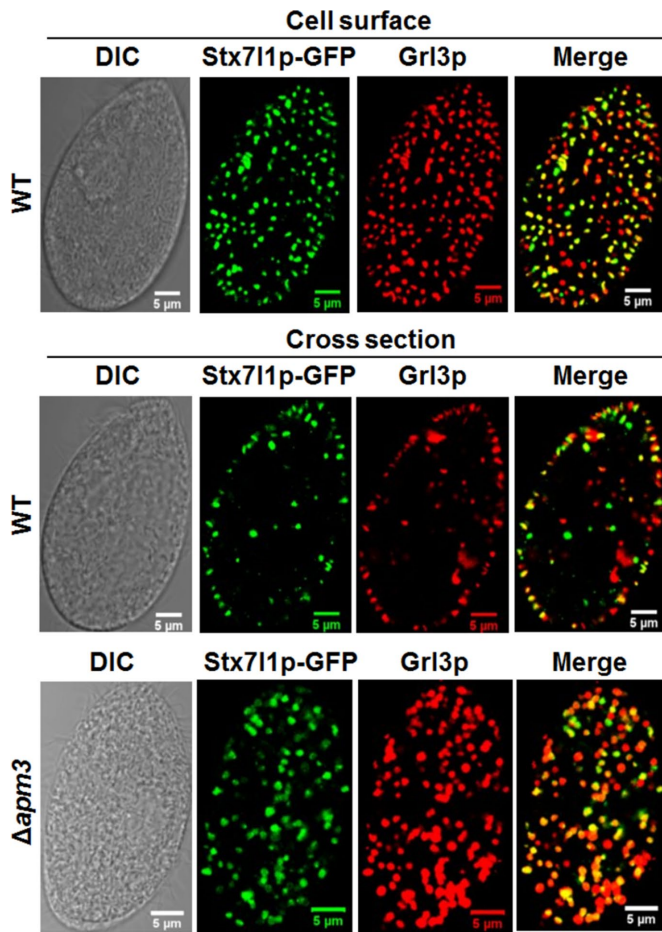


**FIGURE 5:** *T. thermophila* STX7L1 has a mucocyst-related expression profile. The gene encoding STX7L1 is coregulated with mucocyst-associated genes SOR4, GRT1, GRL3, and APM3. Expression profiles were downloaded and normalized as in Figure 1.

example, if it is rapidly secreted—or that it accumulates in a form or compartment that is unstable during fixation or is rapidly turned over within the cell. Unfortunately, live-cell imaging of Grt1p-GFP was precluded because this fusion protein was poorly expressed (unpublished data). We therefore turned to live-cell imaging of a second protein in the GRT family, called induced upon granule regeneration 1p (Igr1p), for which a GFP-fusion is well expressed (Haddad *et al.*, 2002; Bowman *et al.*, 2005b). Both Grt1p and Igr1p require Sor4p for their targeting to mucocysts (Briguglio *et al.*, 2013) and are therefore likely to follow the same trafficking pathway.

We expressed GFP-tagged copies of Igr1p and Grl3p to observe in live wild-type and  $\Delta stx711$  cells. In wild-type cells, Grl3p-GFP and Igr1p-GFP both accumulate in mucocysts (Figure 7, C and D, top). Although Grl3p-GFP is properly localized, its expression evidently perturbs normal organized assembly of mucocyst contents, judging by the fact that mucocysts synthesized in these cells are spherical rather than elongated (Figure 7C, top). In live  $\Delta stx711$ , Grl3p-GFP is found in cytoplasmic puncta (Figure 7C, bottom left), similar to the result in fixed cells (Supplemental Figure S5C, bottom right). Some of these Grl3p-GFP puncta are arrayed around large vesicles (Figure 7C, boxed area in bottom middle). These may be food vacuoles, and this feature was not seen in fixed cells. Most significantly, unlike Grt1p in fixed cells, Igr1p-GFP in live  $\Delta stx711$  could be visualized in cytoplasmic puncta (Figure 7D, bottom). This raised the question of whether Grl3p and Igr1p were accumulating in the same vesicles, which we addressed by simultaneously visualizing Igr1p-GFP and endogenous Grl3p in fixed cells.

In wild-type cells, Igr1p-GFP extensively colocalized with endogenous Grl3p in mucocysts (Figure 8, top). Remarkably, Igr1p-GFP in  $\Delta stx711$  showed greatly reduced colocalization with Grl3p (Figure 8, middle). Thus, in the absence of Stx711p, two mucocyst cargo proteins primarily inhabit two distinct populations of vesicles. To assess the specificity of this result, we repeated the coexpression and analysis in  $\Delta apm3$  cells. In that mutant background, Grl3p-GFP and Igr1p-GFP showed strong colocalization, similar to wild type (Figure 8, bottom). Thus colocalization of the two classes of mucocyst proteins depends on Stx711p but not AP-3.



Proportion (M1) of Stx711p-GFP co-localized with Grl3p

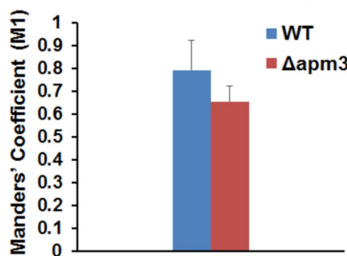


**FIGURE 6:** Stx711p-GFP localizes to immature and mature mucocysts. Cells after 3 h of Stx711p-GFP induction with 2 μg/ml CdCl<sub>2</sub> at 30°C were fixed and immunolabeled to localize Grl3p (mAb5E9) together with Stx711p-GFP. Stx711p-GFP signal overlaps extensively with that of Grl3p, appearing as linear arrays of fluorescent puncta corresponding to docked mucocysts (top). In cross sections of the same cells, the mucocysts appear elongated (middle). In Δapm3 cells, Stx711p-GFP shows extensive colocalization with Grl3p in cytoplasmic vesicles (bottom). Images are single slices, for clarity. Scale bars, 5 μm. The extent of overlap between Stx711p-GFP and Grl3p was quantified and is shown at the bottom; 25 nonoverlapping optical sections were used for each sample. M1 values for wild type: mean, 0.792; SD = 0.131; for Δapm3: mean, 0.65; SD, 0.066; *p* < 0.05 as determined by one-tailed *t* test. For Pearson's correlation analysis of the same data, see Supplemental Figure S7D.

#### Δstx711 cells accumulate aberrant cytoplasmic dense core vesicles containing mucocyst core proteins

To visualize the vesicles formed in Δstx711, we fixed cells and viewed thin sections by electron microscopy. The Δstx711 cells contained

cytoplasmic vesicles with granular contents, not seen in wild type (Figure 9A). Because GRL proteins constitute the major components of mucocyst cores, such vesicles were strong candidates for the Grl3p-containing vesicles seen by immunolabeling in Δstx711.

To confirm that these vesicles were related to mucocysts, we used correlative light-and-electron microscopy (CLEM). Δstx711 cells expressing Grl3-GFP were fixed and visualized to identify GFP-containing vesicles. Selected cells were then embedded, sectioned, and viewed by electron microscopy (EM) in a way that allowed mapping of fluorescent puncta onto the EM image. This analysis confirmed that the granular vesicles seen by EM indeed contained Grl3p (Figure 9C). Measurement of vesicles in micrographs of Δstx711 and Δapm3 showed that the vesicle diameter in Δstx711 was ~50% that in Δapm3 (Figure 9B). This size difference suggests that Stx711p may be required for homotypic and/or heterotypic fusion during formation of immature mucocysts. In comparison, wild-type mature mucocysts are ~0.2 × 0.9 μm. Many of the vesicles seen by CLEM contained a thin peripheral layer of more electron-dense material, which was sometimes localized at one pole of the vesicle (Figure 9C, arrowheads). This layer was less obvious in samples prepared for conventional EM (Figure 9A). The difference may be the result of fixation conditions or reflect the presence of Grl3p-GFP in the cells prepared for CLEM. However, some of the arrested mucocyst intermediates in both Δapm3 and Δstx711 cells prepared for conventional EM also showed peripheral electron density (Supplemental Figure S6), suggesting that this feature does not depend on the presence of the GFP-tagged protein.

Taken together, our results suggest that Stx711p is a determinant for a fusion event that involves an endosomal compartment. Our data further suggest that the fusion step is necessary for efficient delivery of Igr1p and Grl3p to a single class of vesicles, which, in wild-type cells, constitute precursors to mature mucocysts.

## DISCUSSION

We set out to test whether the elaborate secretory vesicles in ciliates could be considered a new class of LROs. Mucocyst formation in *T. thermophila* relies on the VPS10/sortilin family receptor Sor4p. However, the *SOR4* gene arose during an expansion of this gene family within ciliates and is therefore not orthologous to sortilins in other eukaryotes (Briguglio *et al.*, 2013). Here we asked whether the AP-3 complex, each of whose subunits is encoded by a single gene in *T. thermophila*, was also required for mucocyst formation. Because knocking out the μ subunit was sufficient to disrupt AP-3 function in *S. cerevisiae* and *Drosophila melanogaster*, we took the same approach in *Tetrahymena* by targeting the *APM3* gene. The cells showed no growth defects, demonstrating that *APM3* is nonessential, but were blocked in mucocyst maturation. Specifically, although both cargo proteins (of the GRL and GRT families) and processing enzymes (Cth3p and Cth4p) were delivered to arrested mucocyst intermediates, the biochemical and morphological maturation of those intermediates was largely blocked. In wild-type cells, delivery of Grt1p and Cth3p to mucocysts depends on Sor4p; for Grt1p, in particular, this appears to be an absolute requirement (Briguglio *et al.*, 2013). Thus the accumulation of both Grt1p and Cth3p in the Δapm3 immature mucocysts argues strongly that Sor4p-dependent cargo sorting is independent of AP-3. Consistent with this, the cytoplasmic tail of Sor4p lacks any canonical AP-3 sorting motif (unpublished data). Results in *Toxoplasma* also suggest that the sole sortilin receptor in that organism does not interact with AP-3 but instead does with AP-1 (Sloves *et al.*, 2012). *T. thermophila* encodes two AP-1 complexes. We targeted the individual μ subunits (*APM1A* and *APM1B*) for disruption. One of these (*APM1A*) was essential, that is,

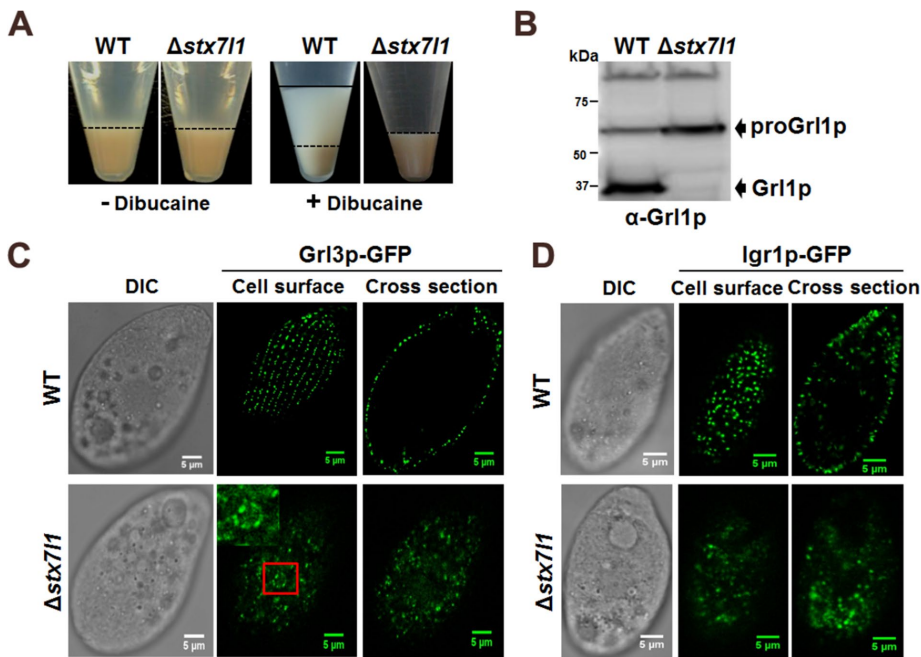


**FIGURE 7:** *STX7L1* is required for mucocyst formation. (A) Dibucaine-triggered mucocyst discharge in WT and  $\Delta stx7/11$  was measured using the same assay as in Figure 2A. In contrast to WT, stimulated  $\Delta stx7/11$  cells do not release a flocculent layer. Left, unstimulated WT and  $\Delta pm3$ . (B)  $\Delta stx7/11$  is blocked in proGr1 processing. Whole-cell lysates of WT and  $\Delta stx7/11$  were resolved by SDS-PAGE (4–20%), electroblotted onto PVDF, and probed with an antibody against Gr1p, which undergoes proteolytic processing during mucocyst maturation. In WT lysates, Gr1p accumulates predominantly in its fully processed form. In  $\Delta stx7/11$  lysates, Gr1p remains entirely as the unprocessed precursor (proGr1p). (C) *Stx71p* is required for normal mucocyst biogenesis. Live-cell images showing Gr13p-GFP in WT (top) and  $\Delta stx7/11$  (bottom). Gr13p-GFP accumulates in docked mucocysts at the cell periphery in WT cells (top; surface and cross sections). In  $\Delta stx7/11$ , Gr13p-GFP signal is chiefly found in cytoplasmic puncta (bottom, surface and cross sections), including puncta at the periphery of large vesicles that may be food vacuoles (highlighted with a box; magnified in the top left inset). Scale bars, 5  $\mu$ m. (D) *Igr1p*-GFP, a mucocyst cargo protein, accumulates in cytoplasmic vesicles in  $\Delta stx7/11$ . *Igr1p*-GFP, after 4 h of induced expression with 1  $\mu$ g/ml CdCl<sub>2</sub> in S medium at 30°C, accumulates in docked mucocysts in WT cells (top) but is found in cytoplasmic puncta in  $\Delta stx7/11$  (bottom). Images are of GFP fluorescence in live, immobilized cells. Scale bars, 5  $\mu$ m.

we integrated a drug-resistance cassette at the *APM1A* locus but could not significantly reduce the level of *APM1A* transcript even after extended passaging in the selective drug. The simplest explanation is that cells with reduced numbers of *APM1A* copies in the polyploid macronucleus have strong growth defects and therefore cannot be selected. The disruption of *APM1B* in contrast had no growth defect and also no effect on mucocyst formation. The question remains open as to whether AP-1A plays a role in mucocyst biogenesis and specifically in sortilin-dependent sorting.

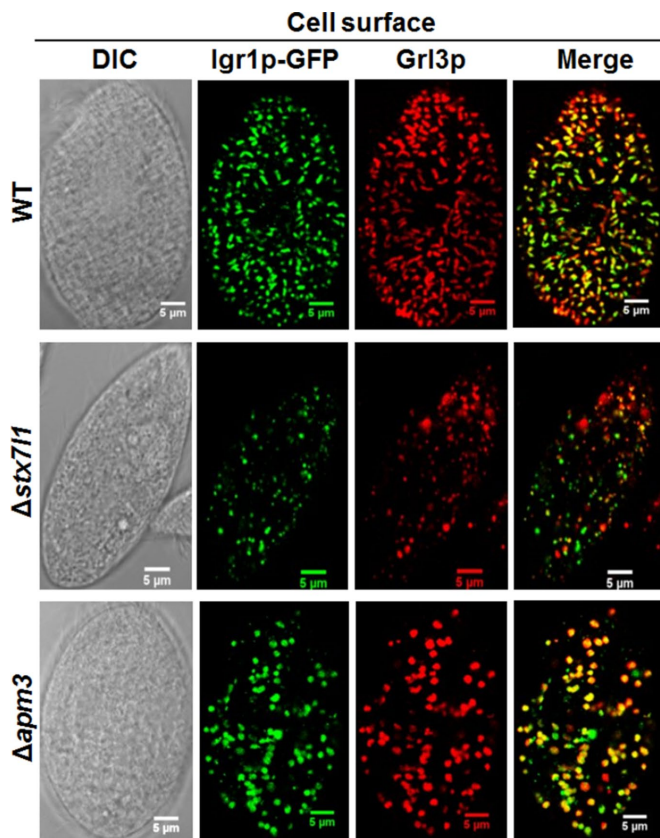
Our finding that not only AP-1A but also AP-2 and AP-4 appear to be essential genes in *T. thermophila* is interesting, in that AP-2 has not previously, to our knowledge, been reported to be essential for cell viability in any organism. Although AP-2 is clearly required for embryonic development in animals, it does not appear to be essential at the level of autonomous cell viability (Motley et al., 2003). The AP-3 complex, nonessential in *Tetrahymena*, is also nonessential in many other lineages and has been entirely lost in some apicomplexans (Nevin and Dacks, 2009).

Based on the roles of AP-3 in other organisms in sorting membrane protein cargo (Odorizzi et al., 1998), AP-3 in *Tetrahymena* is likely to deliver membrane proteins that are required during mucocyst maturation. Our results indicate that factors missing from im-

mature mucocysts in  $\Delta pm3$  are required for cathepsin Cth3p to process proGr1 proteins. These factors may be ion transporters. Mucocyst maturation requires a specific vATPase, as shown by the disruption of one of the six paralogous vATPase  $\alpha$ -subunits, a gene that is coexpressed with AP-3 (unpublished data). Similarly, the maturation of the homologous secretory organelles in the ciliate *Paramecium tetraurelia*, called trichocysts, relies on a trichocyst-specific vATPase (Wassmer et al., 2006). Of interest, although the action of a vATPase is to transport protons from the cytosol, the trichocyst lumen does not appear to be acidic (Lumpert et al., 1992; Garreau de Loubresse et al., 1994). This suggests that the proton gradient is spent to drive transport of other ions—for example, sodium or calcium—and there is indirect evidence that luminal calcium must be carefully controlled during proGr1 processing in *Tetrahymena* (Verbsky and Turkewitz, 1998). AP-3-dependent targeting of ion transporters to the mucocyst membrane would be similar to the role of AP-3 in delivering chloride and zinc transporters to synaptic vesicles in mammalian neurons (Salazar et al., 2004a,b), sucrose transporter4 to vacuoles in *Arabidopsis* (Wolfenstetter et al., 2012), a CIC-3-related chloride channel in *C. elegans* (Hermann et al., 2012), and the OCA2 chloride transporter to melanosomes in melanocytes (Sitaram et al., 2012).

In wild-type *Tetrahymena*, only morphologically mature mucocysts are seen docked at the plasma membrane, ready to undergo exocytosis. Of interest, some  $\Delta pm3$  immature mucocysts are docking competent, suggesting that maturation of the membrane (to achieve docking competence) and core maturation are not tightly coupled. However, because  $\Delta pm3$  mucocysts retain some proGr1p processing, the observed docking could also reflect a low level of maturation in both compartments.

The second gene we identified as essential for mucocyst formation is *STX7L1*, a homologue to syntaxins that function in vacuole biogenesis in yeast and LRO biogenesis in mammals. *Tetrahymena* syntaxin *Stx71p* localizes to both immature and mature mucocysts and is required for mucocyst formation, as judged by the defects in cells lacking this nonessential gene. The  $\Delta stx7/11$  cells appear to accumulate two distinct mucocyst precursors. The first are vesicles that resemble those in  $\Delta pm3$  cells, containing granular contents with no observable organization. CLEM analysis confirms that these vesicles contain Gr13p-GFP. The vesicles are distinctly smaller than those in  $\Delta pm3$ , and this size difference suggests that  $\Delta stx7/11$  vesicles fail to undergo homotypic and/or heterotypic fusion that occurs during normal mucocyst formation. In addition, the  $\Delta stx7/11$  vesicles, unlike those in  $\Delta pm3$ , never appear docked at the plasma membrane. The second class of mucocyst precursors to accumulate in these cells have thus far only been detected at the level of light microscopy by visualizing a protein in the GRT family, *Igr1p*-GFP. In wild-type and  $\Delta pm3$  cells, *Igr1p*-GFP accumulates exclusively in mature and immature mucocysts, respectively. In striking contrast, most



**Proportion (M1) of Igr1p-GFP co-localized with Grl3p**

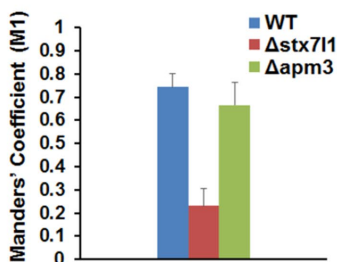


**FIGURE 8:** Grl3p and Igr1p-GFP show only limited co-localization in  $\Delta stx711$ . WT,  $\Delta stx711$ , and  $\Delta apm3$  cells expressing Igr1p-GFP, as in Figure 7D, were fixed and immunolabeled to localize Grl3p (mAb 5E9, followed with Texas red-coupled rabbit anti-mouse). In the WT background, Igr1p-GFP (green) colocalizes extensively with Grl3p (red) within docked mucocysts (top). Similarly, extensive colocalization is seen in  $\Delta apm3$  cells (bottom). In striking contrast, the majority of the Grl3p and Igr1p-GFP signals are nonoverlapping in  $\Delta stx711$  cells (middle). The extents of overlap were quantified and are shown at the bottom; 25 nonoverlapping optical sections were used in each cell line. Scale bars, 5  $\mu$ m. Images are single optical slices. M1 values for WT: mean, 0.743; SD, 0.056; for  $\Delta stx711$ : mean, 0.23; SD, 0.073; for  $\Delta apm3$ : mean, 0.664; SD, 0.115;  $p < 0.01$  as determined by one-tailed t test. For Pearson's correlation analysis of the same data, see Supplemental Figure S7E.

Igr1p-GFP in  $\Delta stx711$  cells appears in puncta that lack the mucocyst core protein, Grl3p. The appearance of these Igr1p-GFP-containing vesicles in  $\Delta stx711$  is consistent with the idea that this syntaxin is required to deliver GRT-family proteins to a secretory compartment containing GRL proteins. Note that a small fraction of Igr1p-GFP

colocalizes with Grl3p-GFP in  $\Delta stx711$ , which may be due to the fact that Igr1p-GFP is overexpressed in these cells. Consistent with this interpretation, we cannot detect any endogenous Grt1p in the Grl3p compartment in these cells.

On the basis of these data, we hypothesize that Stx711p is a member of a fusogenic SNARE complex required for the critical heterotypic fusion event that unites GRL and GRT proteins in the same compartment, the immature mucocyst. A heterotypic fusion event during the formation of secretory organelles in the ciliate *P. dubius* was inferred based on electron microscopy more than two decades ago (Peck et al., 1993). The role of Stx711p in secretory organelle biogenesis is likely to be conserved in *P. tetraurelia*, in which we could identify a likely orthologue via BLAST search (XP\_001454180.1). This gene was not included in a previous survey of *Paramecium* syntaxins (Kissmehl et al., 2007). Of interest, using PSI-BLAST, we also detected a single homologue in the apicomplexan *Babesia bigemina*. Because *T. thermophila* STX7L1 was returned as the top hit by a reciprocal PSI-BLAST, the *Babesia* gene is likely to be an orthologue. This raises the possibility that orthologous syntaxins are involved in LRO biogenesis in that sister lineage within alveolates. The very deep branching of the ciliates from the apicomplexans, as well as perhaps the fast evolution of ciliate genes (Zufall et al., 2006), has made it challenging to detect homologous features between these groups with regard to secretory organelle biogenesis, and so discovery of a shared syntaxin may represent a new window onto the evolution of secretion in alveolates.

## MATERIALS AND METHODS

### Cells and culture conditions

*T. thermophila* strains used in this study are shown in Supplemental Table S1. Strains described as wild type in the text refer to CU428.1, which is wild type with respect to mucocyst formation. Cells were grown at 30°C with constant shaking at 99 rpm in SPP medium (2% proteose peptone, 0.2% dextrose, 0.1% yeast extract, 0.003% ferric EDTA). To reduce autofluorescence in food vacuoles, the cells were transferred to S medium (0.2% yeast extract plus 0.003% iron EDTA) for 2 h before imaging. All reagents were from Sigma Chemical Co. unless otherwise indicated. For the experiments, cell cultures were grown to medium density (log phase:  $[1.5\text{--}3.0] \times 10^5$  cells/ml). Culture densities were measured using a Z1 Coulter Counter (Beckman Coulter).

### Generation of STX7L1- and APM3-knockout strains

The STX7L1 (Tetrahymena Functional Genomics Database THERM\_00420770) and APM3 (THERM\_00572100) macronuclear open reading frames (ORFs) were replaced with the neo4 drug-resistance cassette (Mochizuki, 2008) via homologous recombination with the linearized constructs pSTX7L1MACKO-neo4 and pAPM3MACKO-neo4, respectively. The constructs contain a neo4 construct flanked by ~800 base pairs of the genomic regions immediately upstream and downstream of the STX7L1 or APM3 ORFs. To generate the knockout constructs, the genomic regions upstream and downstream of the STX7L1 or APM3 ORFs were PCR amplified with the primers listed in Supplemental Table S2. The PCR-amplified upstream and downstream regions were subsequently subcloned into the SacI/PstI and XhoI/KpnI sites of the neo4 cassette, respectively. The constructs were linearized by digestion with KpnI and SapI and transformed into CU428.1 cells by biolistic transformation.

### Expression of Stx711p-GFP and Igr1p-GFP

The sequences encoding enhanced GFP (minus the stop codon) and STX7L1 were PCR amplified using the primers listed in

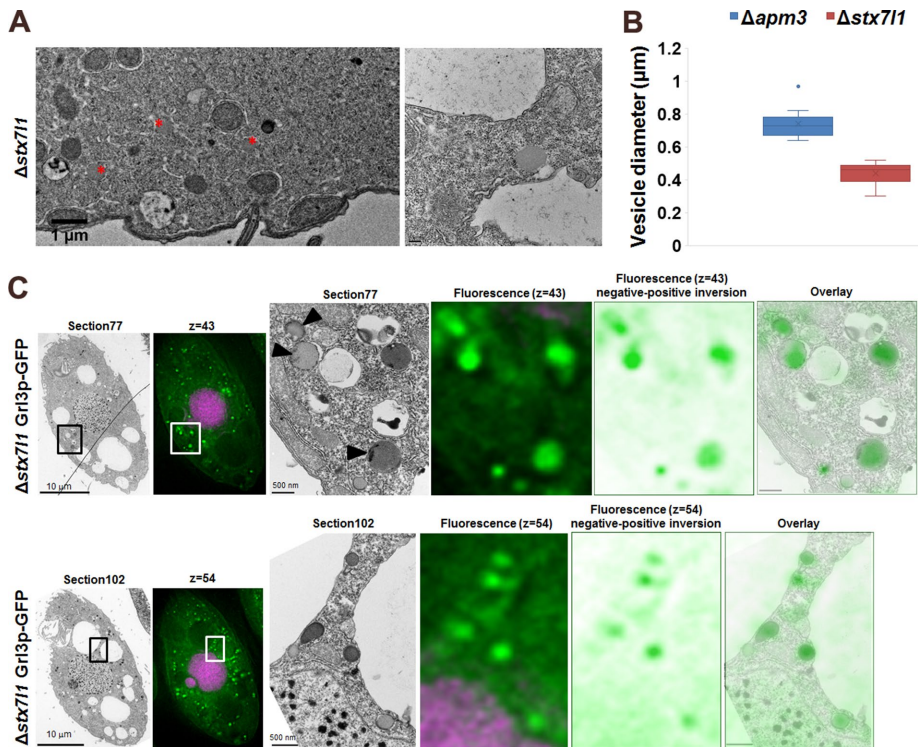


**FIGURE 9:** The  $\Delta stx711$  cells accumulate nondocked cytoplasmic vesicles, smaller than those in  $\Delta apm3$ , with granular, amorphous contents. (A) Electron micrographs of  $\Delta stx711$  cells show distinct vesicles with granular but noncrystalline contents. Scale bars, 1  $\mu\text{m}$  (left), 200 nm (right). (B) Comparison of vesicle diameters (measured from conventional electron micrographs) in  $\Delta apm3$  vs.  $\Delta stx711$  shows an almost twofold difference. We measured 20 randomly chosen vesicles for each cell line. (C) CLEM imaging of  $\Delta stx711$  expressing Grl3p-GFP. Fluorescence images are paired with the corresponding electron micrographs. Left, low-magnification images. Middle, boxed regions shown at high magnification. Right, fluorescence image inverted (negative to positive) and then overlaid on the electron micrograph to show precise mapping of the fluorescence signals onto cellular structures. Grl3p-GFP vesicles lack any visible crystalline organization and often show an electron-dense periphery (arrowheads). Scale bar, 0.5  $\mu\text{m}$ .

Supplemental Table S2 and subsequently cloned into the *ncvB* vector (Bowman *et al.*, 2005a) for blasticidin-based selection using the *PmeI* and *ApaI* restriction sites. The *STX7L1*-GFP construct was linearized with *SfiI* and biolistically transformed into CU428.1 and  $\Delta apm3$ . The *Igr1*-GFP construct, cloned into the *ncvB* vector as previously described (Cowan *et al.*, 2005), was linearized with *SfiI* and biolistically transformed into CU428.1,  $\Delta stx711$ , and  $\Delta apm3$  strains. In these constructs, transgene expression is under the control of the cadmium-inducible metallothionein 1 (*MTT1*) promoter (Shang *et al.*, 2002).

### Endogenous tagging of *GRL3* with GFP

Monomeric superfolder GFP (msEGFP; Pedelacq *et al.*, 2006) was fused at the C-terminus of the *GRL3* (THERM\_00624730) macro-nuclear ORF via homologous recombination using linearized pGRL3-smEGFP-CHX. This construct contains the C-terminal ~850 base pairs of the *GRL3* genomic locus (minus the stop codon) followed by smEGFP, the *BTU1* terminator (Liu and Gorovsky, 1993), the cycloheximide (CHX) drug-resistance cassette (Yao and Yao, 1991), and ~800 base pairs of *GRL3* downstream genomic sequence. The primer sequences used for PCR amplifications are listed in Supplemental Table S2. Wild-type and  $\Delta stx711$  strains were then biolistically transformed with the final construct, pGRL3-smEGFP-CHX, which was first linearized with *SacI* and *KpnI*.

### Expression of Cth3p-GFP and Cth4p-GFP

The sequences encoding *CTH3* (THERM\_00321680) and *CTH4* (THERM\_00445920), omitting the stop codons, and EGFP were PCR amplified using the primers listed in Supplemental Table S2 and subcloned into the *ncvB* vector using the *PmeI* and *ApaI* restriction sites. The *CTH3*-GFP and *CTH4*-GFP constructs were linearized with *SfiI* and biolistically introduced into CU428.1 and  $\Delta apm3$ , and transformants were selected using blasticidin.

### Biolistic transformation

*Tetrahymena* cultures were grown to mid log phase and starved for 18–24 h in 10 mM Tris, pH 7.4. Biolistic transformations were performed as described previously (Chilcoat *et al.*, 1996; Cassidy-Hanley *et al.*, 1997). To select for positive transformants, drug was added 4 h after bombardment to cultures shaken at 30°C. Transformants were selected in paromomycin sulfate (PMS; 120  $\mu\text{g}/\text{ml}$  plus 1  $\mu\text{g}/\text{ml}$   $\text{CdCl}_2$ ), blasticidin (60  $\mu\text{g}/\text{ml}$  plus 1  $\mu\text{g}/\text{ml}$   $\text{CdCl}_2$ ), or CHX (12  $\mu\text{g}/\text{ml}$  plus 1  $\mu\text{g}/\text{ml}$   $\text{CdCl}_2$ ). Drug-resistant transformants were identified after 3–6 d. Transformants were then serially transferred daily in increasing concentration of drug (for PMS and CHX) and decreasing concentrations of  $\text{CdCl}_2$  for at least 2–3 wk before further testing. At least three independent transformants were tested for each line.

### RT-PCR assessment of *STX7L1* and *APM3* disruption

Total RNA was isolated as per manufacturer's instructions using the RNeasy Mini Kit (Qiagen, Valencia, CA). The presence of the *STX7L1* and *APM3* transcripts was assayed by RT-PCR (Multiscribe Reverse Transcriptase Kit; Applied Biosystems, Foster City, CA) using primers (Supplemental Table S2) to amplify ~250 base pairs of each gene. Gene knockouts were confirmed by the continued absence of the corresponding transcripts after 3 wk of growth in the absence of drug selection (four or five serial transfers per week). To confirm that equal amounts of cDNA were being amplified, control RT-PCRs with primers specific for a similarly sized amplicon from the  $\beta$ -tubulin 1 (*BTU1*) gene were run in parallel.

### Live-cell microscopy

Transformants expressing Grl3p-GFP were grown to  $(1.5\text{--}3.0) \times 10^5$  cells/ml in SPP medium, pelleted, and transferred to S medium at 30°C for 2 h before imaging. Cells transformed with *Igr1*p-GFP were grown overnight in SPP medium with 0.1  $\mu\text{g}/\text{ml}$   $\text{CdCl}_2$  and induced with 1  $\mu\text{g}/\text{ml}$   $\text{CdCl}_2$  in S medium at 30°C for 4 h before imaging. Cells transformed with *Stx711*p-GFP were grown in SPP medium with 0.1  $\mu\text{g}/\text{ml}$   $\text{CdCl}_2$ ,  $0.5 \times 10^5$  cells/ml, and induced with 1  $\mu\text{g}/\text{ml}$   $\text{CdCl}_2$  in S medium at 30°C for 3 h before imaging. For immobilization, cells were pelleted and suspended in 3% low-melting agarose (SeaPlaque Agarose; Lonza) dissolved in 10 mM Tris-HCl (pH 7.4) at 37°C, using a resin block to flatten the agarose before hardening.

(Iwamoto *et al.*, 2015; Kobayashi *et al.*, 2016). A 100- $\mu$ l amount of 3% polyethylene oxide (Sigma-Aldrich) in S medium was then layered on top of the agarose gel. This approach results in a thin, flat gel in which many cells are effectively immobilized while showing no visible stress response, for example, autophagosome formation. A Zeiss LSM 880 Confocal Laser Scanning Microscope, 63 $\times$ /numerical aperture (NA) 1.4, was used to collect images (10–20 stacks) along the z-axis at 0.2- to 0.5- $\mu$ m intervals. The images were colored, denoised, and adjusted in brightness/contrast with the Fiji (<http://fiji.sc/Fiji>). Images shown are single slices for clarity.

### Immunofluorescence

Cells were fixed and immunolabeled as described previously (Briguglio *et al.*, 2013). Gr13p and Grt1p were visualized using monoclonal antibody (mAb) 5E9 (1:9) and 4D11 (1:5; Bowman *et al.*, 2005a), respectively, followed by Texas red–conjugated goat anti-mouse antibody (1:100; Life Technologies, Carlsbad, CA). For simultaneous localization of Gr13p with Stx711p-GFP or Igr1p-GFP, cells transformed with Stx711p-GFP or Igr1p-GFP were grown overnight in SPP medium with 0.1  $\mu$ g/ml CdCl<sub>2</sub> and induced with 2  $\mu$ g/ml CdCl<sub>2</sub> in S medium at 30°C for 3 h (4 h for Igr1p-GFP) before fixation. Gr13p was visualized using mAb 5E9 and Texas red–coupled goat anti-mouse immunoglobulin G (IgG) secondary antibody diluted 1:100 in 1% bovine serum albumin blocking solution. For simultaneous localization of Gr13p with GFP-tagged Cth3p or Cth4p, cells transformed with Cth3p-GFP or Cth4p-GFP were grown overnight in SPP medium with 0.1  $\mu$ g/ml CdCl<sub>2</sub> and induced with 2  $\mu$ g/ml CdCl<sub>2</sub> at 30°C for 2 h before fixation. Gr13p was visualized using mAb 5E9, and GFP-tagged Cth3 and Cth4 proteins were visualized using polyclonal anti-GFP antibody (Invitrogen) diluted 1:400. The secondary antibodies, which were added simultaneously to the samples, were Texas red–coupled goat anti-mouse antibody and 488-coupled donkey anti-rabbit IgG (Life Technologies) diluted 1:250. Immunostained cells were mounted with 0.1 mM Trolox to inhibit bleaching and imaged on a Zeiss LSM 880 Confocal Laser Scanning Microscope, 100 $\times$ /NA 1.4, with Zen2.1 confocal software (Zeiss, Thornwood, NY). Images were colored, denoised, and adjusted in brightness/contrast with the Fiji. The simultaneous localization of Grt1p and Gr13p was performed by directly conjugating mAbs 4D11 and 5E9 to Dylight 488 and 650 (Thermo Fisher Scientific, Rockford, IL), respectively, and mixing 1:1 before incubation with samples (Briguglio *et al.*, 2013).

### Colocalization analysis

To estimate the extent of colocalization, Fiji plug-in JACoP was used to calculate the Manders coefficient M1 (Bolte and Cordelières, 2006). M1 represents the ratio of the summed intensities of pixels from the green image, for which the intensity in the red channel is above zero, to the total intensity in the green channel. The images were corrected for noise, and M1 coefficients were calculated by setting the threshold to the estimated value of background. Similarly, Fiji plug-in JACoP was used to calculate Pearson's *r* (Bolte and Cordelières, 2006).

### Measuring docked and undocked mucocysts/ mucocyst-related vesicles

Optical midsections of wild-type and  $\Delta$ apm3 cells that had been immunostained with mAb 5E9 were used to estimate the number of mucocysts or mucocyst-related vesicles that were docked at the plasma membrane, as well as the undocked cohort in the cytoplasm. Each optical midsection was analyzed by using the ImageJ tool Analyze Particles (<http://imagej.nih.gov/ij/>). To count the docked versus undocked vesicles for each cell midsection, we used an approach

similar to that in Briguglio *et al.* (2013). For each cell, a line was traced that was proximal to all fluorescent puncta at the cell periphery. The signal within this trace was defined as nondocked mucocyst-related vesicles, and the signal outside of the trace was defined as the docked cohort.

### Flow cytometry to measure mucocyst cargo protein accumulation

Wild-type,  $\Delta$ apm3, and  $\Delta$ stx7L1 lines were analyzed by flow cytometry. Cells ( $3.5 \times 10^5$ /sample from a culture grown to  $\sim 2.5 \times 10^5$  cells/ml) were fixed and immunolabeled as previously described (Bowman and Turkewitz, 2001; Cowan *et al.*, 2005). For primary antibody incubation, hybridoma supernatants containing mAb 4D11 or 5E9 were diluted 1:2 or 1:3, respectively, for a final volume of 800  $\mu$ l to provide saturating antibody concentrations. Subsequently, Alexa Fluor 488 goat anti-mouse IgG (Invitrogen; 1% in a total volume of 400  $\mu$ l) was used for the secondary incubation. Cells were resuspended in 400  $\mu$ l of Tris-buffered saline. Cells were analyzed on an LSRFortessa 4-15 flow cytometer (BD Biosciences, San Jose, CA) using FACS-*DiVa* software. Excitation was with a 488-nm laser, and the collection filter was a 525/50 band pass filter. The raw FCS files were processed and gated using the FlowJo version 10 platform.

### Transcription profiles

Gene expression profiles were downloaded from the TFGD (<http://tfgd.ihb.ac.cn/>; Miao *et al.*, 2009; Xiong *et al.*, 2011). To plot the graphs, each profile was normalized so that the gene's maximum expression level was set equal to 1.

### Dibucaine stimulation

The dibucaine stimulation assay was performed as described previously (Briguglio *et al.*, 2013).

### SDS–PAGE and Western blotting

To prepare whole cell lysates,  $\sim 3 \times 10^5$  cells were pelleted, washed once with 10 mM Tris, pH 7.4, and precipitated with 10% trichloroacetic acid (TCA). TCA precipitates were incubated on ice for 30 min, centrifuged (18,000  $\times$  g, 10 min, 4°C), washed with ice-cold acetone, centrifuged at 18,000  $\times$  g for 5 min at 4°C, and resuspended in 2 $\times$  SDS–PAGE sample buffer. For Western blots, samples were resolved by SDS–PAGE and transferred to 0.45- $\mu$ m polyvinylidene fluoride (PVDF) membranes (Thermo Scientific). Blots were blocked and probed as previously described (Turkewitz *et al.*, 1991). The polyclonal anti-Gr1p serum and purified anti-GFP mAbs were diluted 1:2,000 and 1:5,000, respectively. Protein was visualized with either ECL horseradish peroxidase–linked anti-rabbit (NA934) or anti-mouse (NA931; Amersham Biosciences, Little Chalfont, United Kingdom), secondary antibody diluted 1:20,000, and SuperSignal West Femto Maximum Sensitivity Substrate (Thermo Scientific).

### Electron microscopy

Cells were grown overnight in SPP medium to mid log phase ( $2.0 \times 10^5$ /ml) and transferred to 10 mM Tris, pH 7.4, for 2 h, fixed in 2.5% glutaraldehyde, 1% sucrose, and 2% osmium at 25°C in 0.1 M sodium cacodylate buffer, and then embedded in epoxy blocks for thin sectioning. Samples were section stained with uranyl acetate and lead citrate. Thin sections were imaged using a Tecnai G2 F30 Super Twin microscope (FEI).

### CLEM imaging

Cells expressing GRL3-GFP were fixed with 2.5% glutaraldehyde (Nacalai Tesque, Kyoto, Japan) for 1 h at room temperature,

washed five times with 100 mM phosphate (pH 7.4), and then embedded in an agarose gel on a glass-bottom dish with an addressing grid (grid size, 175  $\mu\text{m}$ ) on the coverslip (MatTek). Three-dimensional images (50–60 z-stacks  $\times$  0.2- $\mu\text{m}$  intervals) were obtained using an oil immersion objective lens (PlanApoN60xOSC/NA 1.4; Olympus) and processed by deconvolution. EM observation of the same cells was carried out as described previously (Haraguchi *et al.*, 2008). The cells were then postfixed with 1% OsO<sub>4</sub> (Nissin EM, Tokyo, Japan) for 1 h. During sequential dehydration treatments with ethanol, the samples were stained en bloc with 2% uranyl acetate (Wako, Osaka, Japan) in 70% ethanol for 30 min between the dehydration treatments with 70 and 90% ethanol. The epoxy block containing the cells of interest was trimmed according to the address on the grid and sliced to 80-nm sections. Image data were collected by JEM-1400 (JEOL, Tokyo, Japan) with an acceleration voltage of 80 kV. To make a correlation between fluorescence microscopic (FM) and EM images, the aspect ratio of the fluorescence images corresponding to the EM images was adjusted to 1.00–1.09 using PowerPoint. Then a display mode of FM images was inverted from negative to positive using Photoshop. Finally, the FM images were overlaid on the EM images using PowerPoint with 30–40% transparency to generate a single montage image.

### BLAST searches and phylogenetic tree building

Using protein BLAST (blastp), the *T. thermophila* Apm3p amino acid sequence was used to search the nonredundant (nr) database at the National Center for Biotechnology Information ([www.ncbi.nlm.nih.gov](http://www.ncbi.nlm.nih.gov)) to identify homologues in ciliates and other eukaryotic lineages, as documented in Supplemental Table S3. For tree building, the top hits were selected from each lineage, assembled, and aligned with MUSCLE ([www.ebi.ac.uk/Tools/msa/muscle/](http://www.ebi.ac.uk/Tools/msa/muscle/)), and Bayesian trees were constructed with MrBayes (<http://mrbayes.sourceforge.net/>). For Bayesian analysis, the aligned sequence file (in Nexus format) was used to run an analysis using MrBayes until a convergence value 0.01 was reached.

To identify endosomal syntaxins in *Tetrahymena*, the *S. cerevisiae* Vam3p protein sequence was used to search for homologues in the *T. thermophila* nr protein sequence database using position-specific iterated (PSI) BLAST, with the threshold set at 0.01. The top two *T. thermophila* hits were both confirmed as Qa.III.b-SNAREs in the online SNARE-typing database (<http://bioinformatics.mpibpc.mpg.de/snare/index.jsp>). The second of these hits, named STXL1 in this article, returned VAM3 as the top hit by reciprocal PSI-BLAST against the *S. cerevisiae* database.

### ACKNOWLEDGMENTS

We thank Vytautas Bindokas and Christine Labno, as well as Yimei Chen, for assistance in Chicago with light and electron microscopy, respectively, at the respective Core Facilities at the University of Chicago; Lev Tsybin, Beth Richardson, and Joel Dacks (University of Alberta, Edmonton, Canada) and Mark Field (University of Dundee, Dundee, Scotland) for helpful discussion and comments; K. Mochizuki (Institute of Molecular Biotechnology, Vienna, Austria) for NEO4 plasmids, and J. Frankel (University of Iowa, Iowa City, IA) for mAbs 5E9 and 4D11. A.P.T. is indebted to Takako Koujin (Advanced ICT Research Institute, Kobe, Japan) for advice on cell immobilization. This work was supported by Japan Society for the Promotion of Science Kakenhi Grants JP15K07066 (M.I.) and JP26291007, JP25116006, and JP15K21730 (T.H.) and National Institutes of Health Grant GM-105783 (A.P.T.).

### REFERENCES

- Adoutte A, Garreau de Loubresse N, Beisson J (1984). Proteolytic cleavage and maturation of the crystalline secretion products of *Paramecium*. *J Mol Biol* 180, 1065–1081.
- Arvan P, Castle D (1998). Sorting and storage during secretory granule biogenesis: looking backward and looking forward. *Biochem J* 332, 593–610.
- Asensio CS, Sirkis DW, Edwards RH (2010). RNAi screen identifies a role for adaptor protein AP-3 in sorting to the regulated secretory pathway. *J Cell Biol* 191, 1173–1187.
- Becherer KA, Rieder SE, Emr SD, Jones EW (1996). Novel syntaxin homologue, Pep12p, required for the sorting of luminal hydrolases to the lysosome-like vacuole in yeast. *Mol Biol Cell* 7, 579–594.
- Bennett MK, Garcia-Ararras JE, Elferink LA, Peterson K, Fleming AM, Hazuka CD, Scheller RH (1993). The syntaxin family of vesicular transport receptors. *Cell* 74, 863–873.
- Blaby-Haas CE, Merchant SS (2014). Lysosome-related organelles as mediators of metal homeostasis. *J Biol Chem* 289, 28129–28136.
- Bolte S, Cordelières FP (2006). A guided tour into subcellular colocalization analysis in light microscopy. *J Microsc* 224, 213–232.
- Bonifacino JS (2004). Insights into the biogenesis of lysosome-related organelles from the study of the Hermansky-Pudlak syndrome. *Ann NY Acad Sci* 1038, 103–114.
- Bowman GR, Elde NC, Morgan G, Winey M, Turkewitz AP (2005a). Core formation and the acquisition of fusion competence are linked during secretory granule maturation in *Tetrahymena*. *Traffic* 6, 303–323.
- Bowman GR, Smith DG, Michael Siu KW, Pearlman RE, Turkewitz AP (2005b). Genomic and proteomic evidence for a second family of dense core granule cargo proteins in *Tetrahymena thermophila*. *J Eukaryot Microbiol* 52, 291–297.
- Bowman GR, Turkewitz AP (2001). Analysis of a mutant exhibiting conditional sorting to dense core secretory granules in *Tetrahymena thermophila*. *Genetics* 159, 1605–1616.
- Briguglio JS, Kumar S, Turkewitz AP (2013). Lysosomal sorting receptors are essential for secretory granule biogenesis in *Tetrahymena*. *J Cell Biol* 203, 537–550.
- Canuel M, Libin Y, Morales CR (2009). The interactomics of sortilin: an ancient lysosomal receptor evolving new functions. *Histol Histopathol* 24, 481–492.
- Cassidy-Hanley D, Bowen J, Lee JH, Cole E, VerPlank LA, Gaertig J, Gorovsky MA, Bruns PJ (1997). Germline and somatic transformation of mating *Tetrahymena thermophila* by particle bombardment. *Genetics* 146, 135–147.
- Chanat E, Huttner WB (1991). Milieu-induced, selective aggregation of regulated secretory proteins in the trans-Golgi network. *J Cell Biol* 115, 1505–1519.
- Chilcoat ND, Melia SM, Haddad A, Turkewitz AP (1996). Granule lattice protein 1 (Gr1p), an acidic, calcium-binding protein in *Tetrahymena thermophila* dense-core secretory granules, influences granule size, shape, content organization, and release but not protein sorting or condensation. *J Cell Biol* 135, 1775–1787.
- Collins T, Wilhelm JM (1981). Post-translational cleavage of mucocyst precursors in *Tetrahymena*. *J Biol Chem* 256, 10475–10484.
- Cowan AT, Bowman GR, Edwards KF, Emerson JJ, Turkewitz AP (2005). Genetic, genomic, and functional analysis of the granule lattice proteins in *Tetrahymena* secretory granules. *Mol Biol Cell* 16, 4046–4060.
- Cowles CR, Odorizzi G, Payne GS, Emr SD (1997). The AP-3 adaptor complex is essential for cargo-selective transport to the yeast vacuole. *Cell* 91, 109–118.
- Dacks JB, Poon PP, Field MC (2008). Phylogeny of endocytic components yields insight into the process of nonendosymbiotic organelle evolution. *Proc Natl Acad Sci USA* 105, 588–593.
- Darsow T, Burd CG, Emr SD (1998). Acidic di-leucine motif essential for AP-3-dependent sorting and restriction of the functional specificity of the Vam3p vacuolar t-SNARE. *J Cell Biol* 142, 913–922.
- Dennis MK, Mantegazza AR, Snir OL, Tenza D, Acosta-Ruiz A, Delevoye C, Zorger R, Sitaram A, de Jesus-Rojas W, Ravichandran K, *et al.* (2015). BLOC-2 targets recycling endosomal tubules to melanosomes for cargo delivery. *J Cell Biol* 209, 563–577.
- Ding Y, Ron A, Satir BH (1991). A potential mucus precursor in *Tetrahymena* wild type and mutant cells. *J Protozool* 38, 613–623.
- Docampo R, de Souza W, Miranda K, Rohloff P, Moreno SN (2005). Acidocalcisomes—conserved from bacteria to man. *Nat Rev Microbiol* 3, 251–261.
- Docampo R, Jimenez V, Lander N, Li ZH, Niyogi S (2013). New insights into roles of acidocalcisomes and contractile vacuole complex in osmoregulation in protists. *Int Rev Cell Mol Biol* 305, 69–113.

- Docherty K, Steiner DF (1982). Post-translational proteolysis in polypeptide hormone biosynthesis. *Annu Rev Physiol* 44, 625–638.
- Feraru E, Paciorek T, Feraru MI, Zwiewka M, De Groodt R, De Rycke R, Kleine-Vehn J, Friml J (2010). The AP-3 beta adaptin mediates the biogenesis and function of lytic vacuoles in Arabidopsis. *Plant Cell* 22, 2812–2824.
- Gao F, Warren A, Zhang Q, Gong J, Miao M, Sun P, Xu D, Huang J, Yi Z, Song W (2016). The all-data-based evolutionary hypothesis of ciliated protists with a revised classification of the phylum Ciliophora (Eukaryota, Alveolata). *Sci Rep* 6, 24874.
- Garreau de Loubresse N, Gautier MC, Sperling L (1994). Immature secretory granules are not acidic in Paramecium: implications for sorting to the regulated pathway. *Biol Cell* 82, 139–147.
- Gautam R, Novak EK, Tan J, Wakamatsu K, Ito S, Swank RT (2006). Interaction of Hermansky-Pudlak syndrome genes in the regulation of lysosome-related organelles. *Traffic* 7, 779–792.
- Grabner CP, Price CD, Lysakowski A, Cahill AL, Fox AP (2006). Regulation of large dense-core vesicle volume and neurotransmitter content mediated by adaptor protein 3. *Proc Natl Acad Sci USA* 103, 10035–10040.
- Guerrier S, Plattner H, Richardson E, Dacks JB, Turkewitz AP (2017). An evolutionary balance: conservation vs innovation in ciliate membrane trafficking. *Traffic* 18, 18–28.
- Haddad A, Bowman GR, Turkewitz AP (2002). A new class of cargo protein in Tetrahymena thermophila dense core secretory granules. *Eukaryot Cell* 1, 583–593.
- Hannah MJ, Williams R, Kaur J, Hewlett LJ, Cutler DF (2002). Biogenesis of Weibel-Palade bodies. *Semin Cell Dev Biol* 13, 313–324.
- Haraguchi T, Kojidani T, Koujin T, Shimi T, Osakada H, Mori C, Yamamoto A, Hiraoka Y (2008). Live cell imaging and electron microscopy reveal dynamic processes of BAF-directed nuclear envelope assembly. *J Cell Sci* 121, 2540–2554.
- Hermann GJ, Scavarda E, Weis AM, Saxton DS, Thomas LL, Salesky R, Somhegyi H, Curtin TP, Barrett A, Foster OK, et al. (2012). C. elegans BLOC-1 functions in trafficking to lysosome-related gut granules. *PLoS One* 7, e43043.
- Hermann GJ, Schroeder LK, Hieb CA, Kershner AM, Rabbitts BM, Fonarev P, Grant BD, Priess JR (2005). Genetic analysis of lysosomal trafficking in Caenorhabditis elegans. *Mol Biol Cell* 16, 3273–3288.
- Iwamoto M, Koujin T, Osakada H, Mori C, Kojidani T, Matsuda A, Asakawa H, Hiraoka Y, Haraguchi T (2015). Biased assembly of the nuclear pore complex is required for somatic and germline nuclear differentiation in Tetrahymena. *J Cell Sci* 128, 1812–1823.
- Jani RA, Purushothaman LK, Rani S, Bergam P, Setty SR (2015). STX13 regulates cargo delivery from recycling endosomes during melanosome biogenesis. *J Cell Sci* 128, 3263–3276.
- Kantheti P, Qiao X, Diaz ME, Peden AA, Meyer GE, Carskadon SL, Kapfhamer D, Sufalko D, Robinson MS, Noebels JL, et al. (1998). Mutation in AP-3 delta in the mocha mouse links endosomal transport to storage deficiency in platelets, melanosomes, and synaptic vesicles. *Neuron* 21, 111–122.
- Keller P, Simons K (1997). Post-Golgi biosynthetic trafficking. *J Cell Sci* 110, 3001–3009.
- Kissmehl R, Schilde C, Wassmer T, Danzer C, Nuehse K, Lutter K, Plattner H (2007). Molecular identification of 26 syntaxin genes and their assignment to the different trafficking pathways in Paramecium. *Traffic* 8, 523–542.
- Klinger CM, Klute MJ, Dacks JB (2013). Comparative genomic analysis of multi-subunit tethering complexes demonstrates an ancient pan-eukaryotic complement and sculpting in Apicomplexa. *PLoS One* 8, e76278.
- Klopper TH, Kienle CN, Fasshauer D (2007). An elaborate classification of SNARE proteins sheds light on the conservation of the eukaryotic endomembrane system. *Mol Biol Cell* 18, 3463–3471.
- Kobayashi S, Iwamoto M, Haraguchi T (2016). Live correlative light-electron microscopy to observe molecular dynamics in high resolution. *Microscopy (Oxf)* 65, 296–308.
- Kuliawat R, Klumperman J, Ludwig T, Arvan P (1997). Differential sorting of lysosomal enzymes out of the regulated secretory pathway in pancreatic beta cells. *J Cell Biol* 137, 595–608.
- Kumar S, Briguglio JS, Turkewitz AP (2014). An aspartyl cathepsin, CTH3, is essential for proprotein processing during secretory granule maturation in Tetrahymena thermophila. *Mol Biol Cell* 25, 2444–2460.
- Kumar S, Briguglio JS, Turkewitz AP (2015). Secretion of polypeptide crystals from Tetrahymena thermophila secretory organelles (mucocysts) depends on processing by a cysteine cathepsin, Cth4p. *Eukaryotic Cell* 14, 817–833.
- Li W, Zhang Q, Oiso N, Novak EK, Gautam R, O'Brien EP, Tinsley CL, Blake DJ, Spritz RA, Copeland NG, et al. (2003). Hermansky-Pudlak syndrome type 7 (HPS-7) results from mutant dysbindin, a member of the biogenesis of lysosome-related organelles complex 1 (BLOC-1). *Nat Genet* 35, 84–89.
- Liu X, Gorovsky MA (1993). Mapping the 5' and the 3' ends of Tetrahymena thermophila mRNAs using RNA ligase mediated amplification of cDNA ends (RLM-RACE). *Nucleic Acids Res* 21, 4954–4960.
- Lumpert CJ, Glas-Albrecht R, Eisenmann E, Plattner H (1992). Secretory organelles in Paramecium cells (trichocysts) are not remarkably acidic compartments. *J Histochem Cytochem* 40, 153–160.
- Luzio JP, Hackmann Y, Dieckmann NM, Griffiths GM (2014). The biogenesis of lysosomes and lysosome-related organelles. *Cold Spring Harb Perspect Biol* 6, a016840.
- Madeddu L, Gautier MC, Vayssie L, Houari A, Sperling L (1995). A large multigene family codes for the polypeptides of the crystalline trichocyst matrix in Paramecium. *Mol Biol Cell* 6, 649–659.
- Marcusson EG, Horazdovsky BF, Cereghino JL, Gharakhanian E, Emr SD (1994). The sorting receptor for yeast vacuolar carboxypeptidase Y is encoded by the VPS10 gene. *Cell* 77, 579–586.
- Marks MS, Heijnen HF, Raposo G (2013). Lysosome-related organelles: unusual compartments become mainstream. *Curr Opin Cell Biol* 25, 495–505.
- Melia SM, Cole ES, Turkewitz AP (1998). Mutational analysis of regulated exocytosis in Tetrahymena. *J Cell Sci* 111, 131–140.
- Miao W, Xiong J, Bowen J, Wang W, Liu Y, Braguinets O, Grigull J, Pearlman RE, Orias E, Gorovsky MA (2009). Microarray analyses of gene expression during the Tetrahymena thermophila life cycle. *PLoS One* 4, e4429.
- Mochizuki K (2008). High efficiency transformation of Tetrahymena using a codon-optimized neomycin resistance gene. *Gene* 425, 79–83.
- Molinete M, Irminger JC, Tooze SA, Halban PA (2000). Trafficking/sorting and granule biogenesis in the beta-cell. *Semin Cell Dev Biol* 11, 243–251.
- Morlon-Guyot J, Pastore S, Berry L, Lebrun M, Daher W (2015). Toxoplasma gondii Vps11, a subunit of HOPS and CORVET tethering complexes, is essential for the biogenesis of secretory organelles. *Cell Microbiol* 17, 1157–1178.
- Morvan J, Tooze SA (2008). Discovery and progress in our understanding of the regulated secretory pathway in neuroendocrine cells. *Histochem Cell Biol* 129, 243–252.
- Motley A, Bright NA, Seaman MN, Robinson MS (2003). Clathrin-mediated endocytosis in AP-2-depleted cells. *J Cell Biol* 162, 909–918.
- Mullins C, Hartnell LM, Bonifacio JS (2000). Distinct requirements for the AP-3 adaptor complex in pigment granule and synaptic vesicle biogenesis in Drosophila melanogaster. *Mol Gen Genet* 263, 1003–1014.
- Mullock BM, Smith CW, Ihrke G, Bright NA, Lindsay M, Parkinson EJ, Brooks DA, Parton RG, James DE, Luzio JP, et al. (2000). Syntaxin 7 is localized to late endosome compartments, associates with Vamp 8, and is required for late endosome-lysosome fusion. *Mol Biol Cell* 11, 3137–3153.
- Nevin WD, Dacks JB (2009). Repeated secondary loss of adaptin complex genes in the Apicomplexa. *Parasitol Int* 58, 86–94.
- Odorizzi G, Cowles CR, Emr SD (1998). The AP-3 complex: a coat of many colours. *Trends Cell Biol* 8, 282–288.
- Orci L, Ravazzola M, Amherdt M, Madsen O, Vassalli JD, Perrelet A (1985). Direct identification of prohormone conversion site in insulin-secreting cells. *Cell* 42, 671–681.
- Orci L, Ravazzola M, Amherdt M, Perrelet A, Powell SK, Quinn DL, Moore HP (1987). The trans-most cisternae of the Golgi complex: a compartment for sorting of secretory and plasma membrane proteins. *Cell* 51, 1039–1051.
- Orias E, Flacks M, Satir BH (1983). Isolation and ultrastructural characterization of secretory mutants of Tetrahymena thermophila. *J Cell Sci* 64, 49–67.
- Palade G (1975). Intracellular aspects of the process of protein synthesis. *Science* 189, 347–358.
- Peck RK, Swiderski B, Tourmel AM (1993). Involvement of the trans-Golgi network, coated vesicles, vesicle fusion, and secretory product condensation in the biogenesis of Pseudomicrothorax trichocysts. In: *Membrane Traffic in Protozoa*, Greenwich, CT: JAI Press, 1–26.
- Pedelacq JD, Cabantous S, Tran T, Terwilliger TC, Waldo GS (2006). Engineering and characterization of a superfolder green fluorescent protein. *Nat Biotechnol* 24, 79–88.
- Rahaman A, Miao W, Turkewitz AP (2009). Independent transport and sorting of functionally distinct protein families in Tetrahymena dense core secretory granules. *Eukaryot Cell* 8, 1575–1583.

- Raposo G, Marks MS, Cutler DF (2007). Lysosome-related organelles: driving post-Golgi compartments into specialisation. *Curr Opin Cell Biol* 19, 394–401.
- Roder PV, Wong X, Hong W, Han W (2016). Molecular regulation of insulin granule biogenesis and exocytosis. *Biochem J* 473, 2737–2756.
- Rosati G, Modeo L (2003). Extrusomes in ciliates: diversification, distribution, and phylogenetic implications. *J Eukaryot Microbiol* 50, 383–402.
- Salazar G, Love R, Styers ML, Werner E, Peden A, Rodriguez S, Gearing M, Wainer BH, Faundez V (2004a). AP-3-dependent mechanisms control the targeting of a chloride channel (ClC-3) in neuronal and non-neuronal cells. *J Biol Chem* 279, 25430–25439.
- Salazar G, Love R, Werner E, Doucette MM, Cheng S, Levey A, Faundez V (2004b). The zinc transporter ZnT3 interacts with AP-3 and it is preferentially targeted to a distinct synaptic vesicle subpopulation. *Mol Biol Cell* 15, 575–587.
- Satir B (1977). Dibucaine-induced synchronous mucocyst secretion in *Tetrahymena*. *Cell Biol Int Rep* 1, 69–73.
- Shang Y, Song X, Bowen J, Corstanje R, Gao Y, Gaertig J, Gorovsky MA (2002). A robust inducible-repressible promoter greatly facilitates gene knockouts, conditional expression, and overexpression of homologous and heterologous genes in *Tetrahymena thermophila*. *Proc Natl Acad Sci USA* 99, 3734–3739.
- Sitaram A, Dennis MK, Chaudhuri R, De Jesus-Rojas W, Tenza D, Setty SR, Wood CS, Sviderskaya EV, Bennett DC, Raposo G, et al. (2012). Differential recognition of a dileucine-based sorting signal by AP-1 and AP-3 reveals a requirement for both BLOC-1 and AP-3 in delivery of OCA2 to melanosomes. *Mol Biol Cell* 23, 3178–3192.
- Sloves PJ, Delhaye S, Mouveaux T, Werkmeister E, Slomianny C, Hovasse A, Dilezitoko Alayi T, Callebaut I, Gaji RY, Schaeffer-Reiss C, et al. (2012). Toxoplasma sortilin-like receptor regulates protein transport and is essential for apical secretory organelle biogenesis and host infection. *Cell Host Microbe* 11, 515–527.
- Sollner T, Whiteheart SW, Brunner M, Erdjument BH, Geromanos S, Tempst P, Rothman JE (1993). SNAP receptors implicated in vesicle targeting and fusion. *Nature* 362, 318–324.
- Starcevic M, Nazarian R, Dell'Angelica EC (2002). The molecular machinery for the biogenesis of lysosome-related organelles: lessons from Hermansky-Pudlak syndrome. *Semin Cell Dev Biol* 13, 271–278.
- Steiner DF (1998). The proprotein convertases. *Curr Opin Chem Biol* 2, 31–39.
- Stepp JD, Huang K, Lemmon SK (1997). The yeast adaptor protein complex, AP-3, is essential for the efficient delivery of alkaline phosphatase by the alternate pathway to the vacuole. *J Cell Biol* 139, 1761–1774.
- Tanguy E, Carmon O, Wang Q, Jeandel L, Chasserot-Golaz S, Montero-Hadjadje M, Vitale N (2016). Lipids implicated in the journey of a secretory granule: from biogenesis to fusion. *J Neurochem* 137, 904–912.
- Tooze SA (1991). Biogenesis of secretory granules. Implications arising from the immature secretory granule in the regulated pathway of secretion. *FEBS J* 2, 220–224.
- Turkewitz AP (2004). Out with a bang! *Tetrahymena* as a model system to study secretory granule biogenesis. *Traffic* 5, 63–68.
- Turkewitz AP, Madeddu L, Kelly RB (1991). Maturation of dense core granules in wild type and mutant *Tetrahymena thermophila*. *EMBO J* 10, 1979–1987.
- Vayssie L, Skouri F, Sperling L, Cohen J (2000). Molecular genetics of regulated secretion in *Paramecium*. *Biochimie* 82, 269–288.
- Verbsky JW, Turkewitz AP (1998). Proteolytic processing and Ca<sup>2+</sup>-binding activity of dense-core vesicle polypeptides in *Tetrahymena*. *Mol Biol Cell* 9, 497–511.
- Wada Y, Nakamura N, Ohsumi Y, Hirata A (1997). Vam3p, a new member of syntaxin related protein, is required for vacuolar assembly in the yeast *Saccharomyces cerevisiae*. *J Cell Sci* 110, 1299–1306.
- Wasmeier C, Romao M, Plowright L, Bennett DC, Raposo G, Seabra MC (2006). Rab38 and Rab32 control post-Golgi trafficking of melanogenic enzymes. *J Cell Biol* 175, 271–281.
- Wassmer T, Kissmehl R, Cohen J, Plattner H (2006). Seventeen a-subunit isoforms of *paramecium* V-ATPase provide high specialization in localization and function. *Mol Biol Cell* 17, 917–930.
- Wessenberg H, Antipa G (1970). Capture and ingestion of *Paramecium* by *Didinium nasutum*. *J Protozool* 17, 250–270.
- Wolfenstetter S, Wirsching P, Dotzauer D, Schneider S, Sauer N (2012). Routes to the tonoplast: the sorting of tonoplast transporters in *Arabidopsis mesophyll* protoplasts. *Plant Cell* 24, 215–232.
- Xiong J, Lu X, Lu Y, Zeng H, Yuan D, Feng L, Chang Y, Bowen J, Gorovsky M, Fu C, et al. (2011). *Tetrahymena* Gene Expression Database (TGED): a resource of microarray data and co-expression analyses for *Tetrahymena*. *Sci China Life Sci* 54, 65–67.
- Yao MC, Yao CH (1991). Transformation of *Tetrahymena* to cycloheximide resistance with a ribosomal protein gene through sequence replacement. *Proc Natl Acad Sci USA* 88, 9493–9497.
- Zufall RA, McGrath CL, Muse SV, Katz LA (2006). Genome architecture drives protein evolution in ciliates. *Mol Biol Evol* 23, 1681–1687.
- Zwiewka M, Feraru E, Moller B, Hwang I, Feraru MI, Kleine-Vehn J, Weijers D, Friml J (2011). The AP-3 adaptor complex is required for vacuolar function in *Arabidopsis*. *Cell Res* 21, 1711–1722.